Review

Analysis of Permanent Magnet Motors in High Frequency—A Review

Yerai Moreno [1],* , Gaizka Almandoz [1] , Aritz Egea [1] , Beñat Arribas [1] and Ander Urdangarin [2]

[1] Faculty of Engineering, Mondragon Unibertsitatea, 20500 Arrasate-Mondragón, Spain; galmandoz@mondragon.edu (G.A.); aegea@mondragon.edu (A.E.); benat.arribas@alumni.mondragon.edu (B.A.)

[2] ORONA EIC, 20120 Hernani, Spain; aurdangarinl@orona-group.com

* Correspondence: ymoreno@mondragon.edu; Tel.: +34-664-299-159

Abstract: Electric drives consume a great amount of the world's energy, and it will keep increasing due to the electromobility trend. Thus, the efficiency of electric drives must be improved to reach the desired sustainability goal. The Silicon Carbide devices contribute to this objective due to their high working frequency and lower switching losses. However, working at higher frequencies may bring serious Electromagnetic Compatibility (EMC) problems, as well as insulation stress and higher bearing currents. Hence, it is important to have an electrical machine electrical equivalent circuit model to predict the electromagnetic interference levels. This review summarizes the current state of the art in electrical machine modeling and analysis in high frequency. The main analysis tools as Finite Element Methods, analytic and measurement-based tools are compared in their application on high-frequency electrical machine analysis. Then, different machine high-frequency models are reported, detailing their individual features. Additionally, the influence of the machine design parameters in EMC behavior is outlined for future analysis. All in all, Finite Element analysis is the most accurate tool for high-frequency analysis, provided that mesh size is thinner than the skin depth. It is also concluded that the winding placement is an essential parameter to define the high-frequency behavior of the machine.

Keywords: electromagnetic compatibility; electrical machines; finite element analysis; high frequency; permanent magnet machines

1. Introduction

Typically, an electrical drive consists of a power source, an inverter that applies the desired voltage and frequency to the electrical machine, usually with Pulse Width Modulation (PWM) technique and the electrical motor, as shown in Figure 1. The straight arrows indicate the radiated noise caused by the switching circuits of the converter.
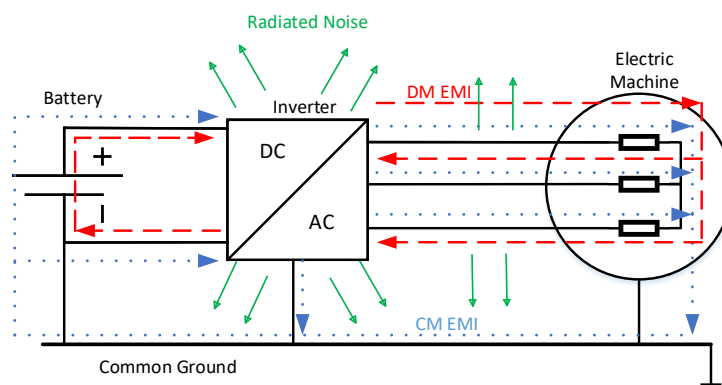

Figure 1. Radiated and Conducted Electromagnetic Interference (EMI) in an electric drive.

The dashed line represents the differential-mode EMI, which is going through one phase and returns across the other phases to the DC bus of the power source. Finally, the dotted line is the common-mode EMI, which goes across the common ground, connecting all elements to the disturbance [1].

Even if PWM technique is the most used control technique, its pulses generate a Common-mode voltage (CMV) in the output connection to the motor causing diverse problems such as leakage current, shaft voltage and bearing currents. The rapid voltage changes (high du/dt) also deteriorate the winding insulation and can cause protection failures in the case of short-circuit or contact defects [2–4]. Moreover, the generated EMI can affect the power source grid and the elements connected to it, for instance, sensors and safety systems in electric cars [5].

Specifically, bearings are affected by the CMV variations, as leakage currents flow through them [6,7]. Those currents damage the bearings, and together with the winding insulation damage due to voltage stress, the reliability and lifetime of the complete electric drive are decreased.

Some solutions are proposed to mitigate this EMI in electric drives. Different inverter typologies and modulation algorithms are proposed to reduce CM voltage [1,6,8]. Filters and other types of add-ons, such as shields or insulation are also widely used to avoid EMI flowing to the power grid as shown in [6,9–11], but they increase the cost of the drive, as well as the volume and the weight as they are bulky and heavy. Hence, those factors can reduce considerably the competitiveness of the final product on the market, for example, in the electric car.

Thus, to reduce the development cost of the product, an EMI strategy-based design should be added early in the product development cycle to reduce costs and achieve the best solution. Consequently, understanding and predicting EMI noise using high-frequency models during the design stage is essential to manage EMI problems.

According to the literature, the most extended modeling techniques for representing the behavior of electrical machines in high-frequency are based on electrical equivalent circuits or Lumped Parameter Models (LPM). These models consist of electrical circuits that comprise several resistances, inductances, and capacitances. The values of this electrical parameters can be obtained applying different procedures. For instance, by experimental measurements [12–36], by analytical calculations considering the main design parameters [11,37–50], by Finite Element Method (FEM) [28,39,51–70] or even by hybrid methods [71–73]. The High-Frequncy LPM models are developed for many purposes in the literature. For example, to analyze the influence of the winding placement and the winding connection on the bearing currents [32,57], to analyze the common-mode currents [73] or to analyze the over-voltages at motor terminals due to modulated supplying voltages [61]. Although all LPM approaches share the same basis, there are many diversified proposals for accounting for different high-frequency phenomena. In addition, as aforementioned, the calculation of the LPM parameters can be faced in different manners. Therefore, it is identified a lack of a comprehensive review about the analysis tools and methodologies for the study of electrical motors in high frequency, identifying the advantages and drawbacks of the main proposals that can be found in the literature.

As stated before, the final objective is an EMI reduction strategy-based design for electrical machines. To reach that objective, in this paper a comprehensive review of high-frequency behavior of electrical motors is proposed, covering the high-frequency phenomena, the tools available to analyze them accurately and the different existing high-frequency models. Additionally, apart from modeling the machine behavior, it is important to know which design parameters affect the EMC behavior of the motor and how they impact on it, as this is the key to the EMC design optimization. Thus, a review of the influence of different design parameters on the high-frequency behavior of the electrical machine is also collected in this paper. It is concluded that the FEM is the most accurate tool to analyze the high-frequency phenomena in these devices. Nevertheless, there are some analytical methods that may be used, especially for capacitance calculation. It is

also found that the most influential design parameter is the winding placement and the impregnation amount, at least for CM currents. However, more research is needed in this area to obtain a valid, broad conclusion for a global EMC optimization design.

The structure of the paper is the following. In Section 2, the main high-frequency phenomena that arise in electrical machines are described. This paper is focused on conducted EMI, so the radiated EMI are out of the scope of this work. Then, in Section 3, the three main analysis tools are described and the benefit of each method is outlined, presenting different cases found in the literature. In Section 4, the modeling of electrical motors is discussed, showing the main models published up to date, with their particular details and differences. In Section 5, the influence of some design parameters on the EMC performance of electrical machines is analyzed. Finally, in Section 6, the main conclusions are outlined and the future challenges are pointed out for a proper EMC oriented design.

2. High-Frequency Phenomena in Electrical Machines

In low-frequency operation range the parameters such as resistance and inductance hardly depend on the frequency, so they can be considered to be constants. However, in high frequencies, some new phenomena arise leading to variations in these parameters. Thus, as the frequency increases, the resistance increases and the inductance decreases.

Before analyzing any electromagnetic device in high-frequency, a specific frequency range must be defined depending on the application standards, as shown in this International Special Committee on Radio Interference (CISPR) guideline [74]. EMI conducted standards cover the frequency range from 150 kHz to 30 MHz, whereas the radiated standards cover the frequency range of 30 MHz to 100 MHz. However, in most cases, it is difficult to obtain models to achieve good accuracy in the whole range of frequencies, especially beyond 10 MHz [17,20,28,39,51]. Moreover, in [75], it is stated that the model of a transformer is not accurate beyond 10 MHz due to the current coupling between Differential-mode (DM) and Common-mode (CM) paths.

2.1. High-Frequency Phenomena in Conductors

The skin effect is the first phenomenon that arises as the frequency increases. Eddy currents are induced in the current carrying conductor due to the self-created High-Frequency (HF) magnetic field. These Eddy currents cause a non-uniform current density inside the conductor, as the electrons are pushed to the outer region of the conductor. This way, the effective cross-section of the conductor is reduced with the frequency, as the current flows only in the skin depth of the conductor (see Figure 2). The skin depth can be computed applying the next well-known analytical expression:

$$\delta = \sqrt{\frac{2}{\omega \mu \sigma}} \tag{1}$$

where ω is the current pulsation, μ is the medium permeability and σ is the conductivity. According to Equation (1), it can be deduced that the higher the frequency is, the thinner the skin depth is.

This surface distribution of the current increases the resistance and decreases the inductance due to the flux distribution inside the conductor. The skin effect is a local effect in each conductor, independent from the neighboring ones, so it can be analyzed simplifying the problem to a single conductor [76,77]. As it depends on the frequency and geometry, it can be mitigated using a smaller conductor diameter than the skin depth.

The neighboring effect between the conductors comprising a coil is defined as the proximity effect, and it is far more influential than the skin effect [52]. The basis is similar to the skin effect, but it considers the effect of induced Eddy currents in a conductor due to the high-frequency magnetic field created by the neighboring conductors. Thus, this phenomenon depends on the relative position between conductors and can be mitigated using windings with parallel strands or Litz wires, although they are complex to manufacture and

they can generate unbalanced current distribution across the strands [78]. The distortion caused by this effect in the current density distribution of an electrical machine coil is shown in Figure 3. When those effects get together, the effective cross-section of a wire decreases further, leading to a higher resistance increase [55,58].
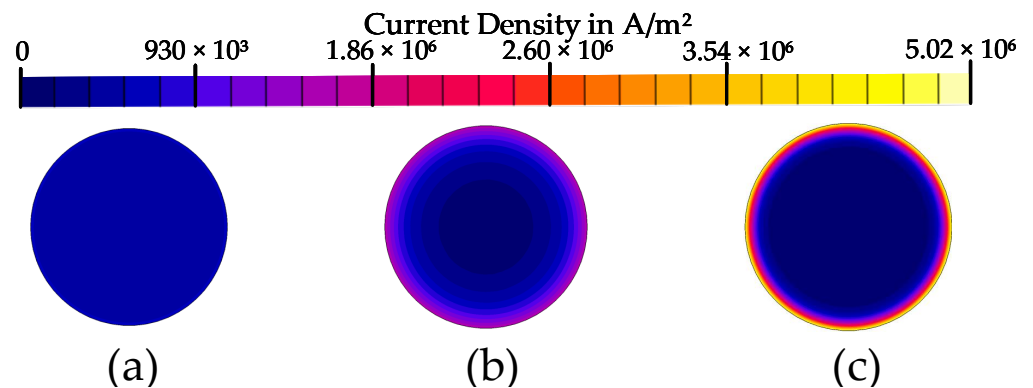

Figure 2. Skin effect in a conductor of 2 mm of diameter. (**a**) 1 kHz. (**b**) 100 kHz. (**c**) 1 MHz.
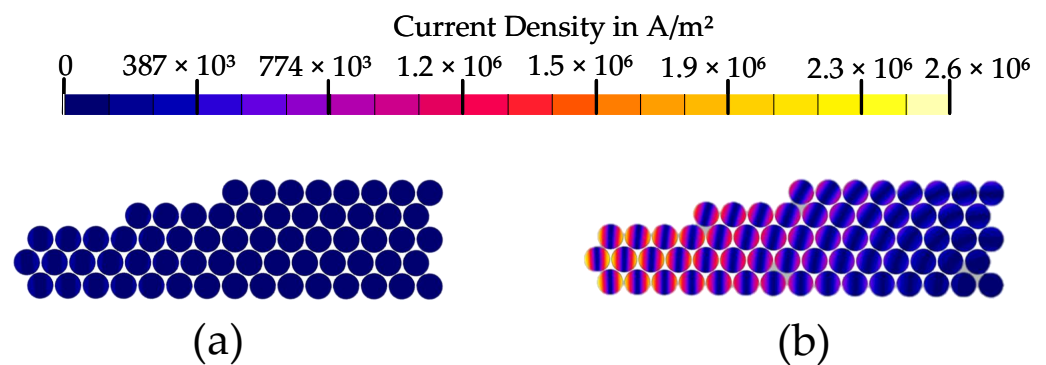

Figure 3. Proximity effect in a middle slot of a machine. (**a**) 1 kHz (**b**) 10 kHz.

2.2. High-Frequency Phenomena in Magnetic Cores

Regarding the magnetic core of electrical machines, in this region also demonstrates some high-frequency phenomena that might have a significant influence on the motor behavior. Generally, the stator and the rotor magnetic cores are laminated and made of electrical steel sheets to limit the Eddy currents induced by alternating magnetic fields, reducing the magnetic losses. However, above a certain frequency, the effect of eddy current is significant despite the insulation given by the lamination, because the skin depth becomes thinner than the thickness of the sheets. The induced Eddy currents creates a shielding effect inside the electrical sheets that push the magnetic flux out of the iron core, leading to a decrease in the relative permeability of the magnetic material, and so in the value of the inductance [52,58,59]. The threshold frequency of this transition depends on the thickness of each steel sheet and its resistivity [24,55,58].

Kohji Maki et al. created a one-slot 2-D model to simulate a bulk iron core and a 3-D model to represent a laminated iron core. In the case of the laminated iron core, the inductance decreases less than in the bulk core since the magnetic flux is not completely pushed out of the laminated core. It also happens at a higher frequency. On the other hand, the resistance increases more in the laminated core, as the surface area where Eddy current flows is larger and the proximity effect between sheets increases the eddy currents in the core. It should be noted that the non-linearity of the magnetic saturation of iron core is neglected for those simulations, as well as the displacement current term, which is negligible at least below 1 GHz [55].

2.3. Parasitic Capacitances

At low frequency, the influence of parasitic capacitances is negligible as their impedance is commonly large. Nevertheless, as the working frequency increases, the impedance of parasitic capacitances gets lower, leading to new current flow paths inside the motor. This might affect considerably to the differential and common-mode impedances, and so to the differential and common-mode currents in the motor [28,58,73,79].

The main parasitic capacitances involved in an electrical motor are shown in Figure 4a. C_{wr} is the winding-to-rotor capacitance, C_b is the bearing capacitance, C_{ws} is the winding-to-stator capacitance, C_{sr} is the stator-to-rotor capacitance, C_{wh} is the winding-to-housing capacitance and C_{wsh} is the winding-to-shaft capacitance.

In the winding, different capacitances appear. C_{ij} is the inter-turn capacitance and C_{pp} is the capacitance between phases that can be neglected if there is a single layer winding in the slot [58]. The complete common-mode (CM) paths are identified in [73]. To calculate the inter-turn capacitances, it is essential to consider the geometry, material and positions of the conductors inside the slot, as well as the thickness and the material of the insulation [43,54].

(a)

(b)
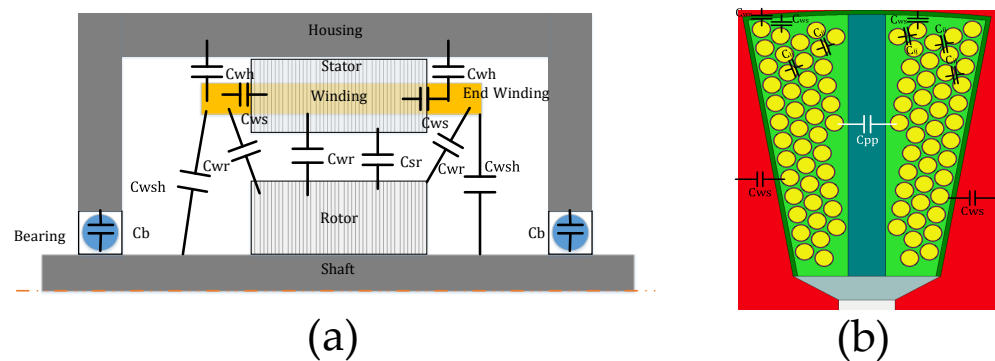
Figure 4. Parasitic Capacitances. (**a**) Motor view. (**b**) Winding turns.

3. Analysis Tools

There are two different ways to analyze an electrical machine in high frequency. The first way is to determine the value of the Lumped Parameter Model (LPM) parameters of the motor by experimental measurements. This method is fairly the most used in the literature [12–36]. It is a practical method that achieves accurate EMC simulation of motor drives. Nevertheless, the manufactured motor is necessary for the measurements, so it is not valid for the design stage before prototyping.

In the second way, an equivalent circuit model or LPM is made so that each circuit constant is calculated with the design parameters of the motor either analytically [11,37–50], by Finite Element Method (FEM) [28,39,51–70] or even with hybrid methods [71–73]. With FEM-based electromagnetic field analysis, the inductance, resistance and capacitance of each turn of winding can be obtained, which are difficult to measure experimentally [55]. In this section, the main analysis tools for the calculation of equivalent circuit parameters are analyzed.

3.1. Finite Element Methods (FEM)

FEM is based on the fundamental laws of electromagnetism described by the Maxwell's equations [80,81].

3.1.1. Analysis of Eddy Currents and Iron Losses

As is well known, the iron losses depend on the frequency, so that the higher the frequency is the higher both the hysteresis and Eddy currents are.

According to some authors, to model those losses accurately, the nonlinear permeability of the magnetic core must be considered [52,61]. In [52], the nonlinear permeability is

considered applying different permeability values to different regions depending on the flux density vector, and the mesh element size is set bellow the wavelength of the PWM excitation frequency. In this way, the non-linearity of the magnetic material BH curve is considered. On the other hand, a linear approximation of the BH curve is proposed in [58], obtaining accurate results.

Even if the high-frequency motor models found in the literature do not mention explicitly how hysteresis and excess losses are calculated, in [82] an improved core loss model is proposed for transformers and machines considering high-frequency and non-sinusoidal supply, which is validated up to 1.6 kHz.

With respect to the model geometry, if working with 2-D models, there are two effects that are not considered, the lamination of the magnetic core and the end effect. Thus, 2-D models tend to overestimate the shield effect in the sheets, resulting in lower iron losses, lower coil inductance and higher resistance [55,66].

In [62] the lamination effect is considered in 2-D models with an equivalent conductivity-D laminated and bulk core simulations are used first. The conductivity of the bulk core is adjusted so that it has equal Eddy losses than the laminated one. The effect of lamination on the magnetic flux distribution can be seen in Figure 5a.

Moreover, in Figure 5b the end effect can be seen, where the end-winding leakage flux causes a local flux density increase in the edge of the tooth-shoe region, generating extra core losses [78].
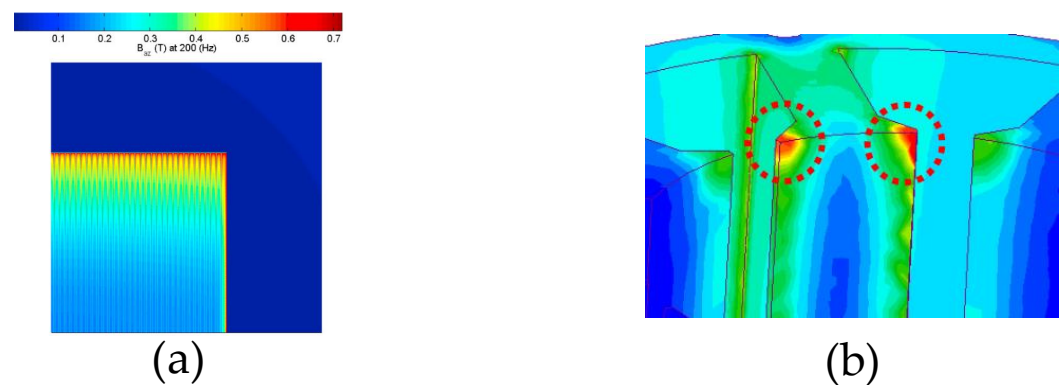
Figure 5. Iron sheet Effects. (**a**) Lamination effect [83]. (**b**) End effect [78].

The stator is a CM current path at high frequency, so its impedance must be calculated. In [83] the impedance of the electrical sheets is calculated for high-frequency transformers, including the two axes. The one parallel to the winding, and the perpendicular one.

3.1.2. Analysis of Coil Conductors

In low-frequency FEM analysis, generally considering the winding coils to be bulk coils might be accurate enough, as the main performance such as the joule losses or the torque capacity do not depend on the supplying frequency. However, when reaching higher frequencies, the detailed modeling of the winding and its fine mesh is essential as the current distribution is not uniform anymore due to skin and proximity effects. The mesh size must be smaller than the skin depth at that frequency to obtain accurate results [63]. Solving a detailed problem might increase the computational load notably, so it is essential to simplify the problem, trying to find a good trade-off between the computational load and the accuracy of the results. Different papers working on this purpose can be found in the literature.

In [72,84] four different FEM models for axial high-speed Permanent Magnet Synchronous Machine (PMSM) are analyzed. Bulk coils and individual conductors with fine mesh, both in 2-D and 3-D domains. In the case of the 3D FEM simulations, the end windings are considered. The most accurate model to calculate the AC losses in the coils is the 3-D complete model, as it considers end, skin and proximity effects. If bulk coils

are used, these effects are not considered. Considering 2D models, usually, even with fine mesh, these models underestimate AC copper losses, as it is stated in [66].

Three methods are proposed to obtain accurate results reducing the computational effort of a 3-D fine mesh:

- Taran et al. propose to use a bulk coil 3-D model with coarse mesh, arguing that it is enough to calculate the magnetic flux density. Then, applying an analytical formulation, the AC copper eddy current losses are calculated. Skin and proximity losses due to neighboring conductors are neglected in this method, as the analyzed conductors are smaller than the skin depth at the calculated frequency of 1.6 kHz. The authors mention that this method may be useful for coreless permanent magnet machines, where the major part of AC component of copper losses is caused by the permanent magnet flux passing over the conductors [72].

- In the case of [84], a 2-D model with detailed conductors and fine mesh is proposed. Then, based on the flux density variation along the active length of the machine in a coarse mesh 3-D model, some coefficients are calculated to account the variation of losses along the end winding and the active length.

- Volpe et al. calculate the flux density for different conductor layers, and then the AC loss is calculated analytically for radial flux machines. If the skin depth is lower than the conductor radius, the flux density must be calculated in different points in each conductor [71].

In Table 1, an overview of the different electromagnetic simulations is shown. Most cases include the rotor in the FEM model, whereas the end winding is just included in 3-D models. The mesh, if mentioned in the articles, is usually lower than the skin depth in the analyzed frequency, to calculate skin and proximity effects accurately. In some cases bulk conductors are used (not each turn conductor), so these effects are not taken into account.

Some cases just mention that iron core properties are considered, without further explanation. However, most cases consider the iron losses, and even the lamination effect, with 3-D models or equivalent 2-D models. Some models use complex permeabilities, and nonlinear BH curves, while others just keep the permeability constant.

The lower part of the table shows some cases where the main objective is to obtain the AC copper losses for high-speed PMSM, with common characteristics with high-frequency models.

Table 1. FEM Electromagnetic simulation comparison.

Case	Frequency Range	Geometry	Mesh	Rotor Model	End Winding	Skin Effect	Proximity Effect	Iron Core
[73]	30–5 M	3-D.1 slot.		x	x [85]		(Bulk turn)	R_{core} & L_{core} [1] [11]
[54] [2]	100–100 M	2-D.1/8 Model.		x		x	x	-
[62]	20–4 M	2-D.1/4 Model.		x			(Bulk turn)	Equivalent σ
[52,86]	10 k	2-D.1/2 Model	$<\delta$	x		x	x	Nonlinear BH
[58]	100–1 M	2-D slot		x		x	x	Complex μ. Linear BH
[61]	0–100 k	2/3-D		x	x	x	x	nonlinear BH and losses
[39]	10–10 M	2-D.1 slot		x		x	x	x
[51]	1 k–10 M	2-D.1 slot				x	x	Constant μ, No lamination
[55]	10 k–20 M	3-D.3 slot	$<\delta$		x	x	x	Constant μ. One sheet
[67]	0–10 M	2-D.1 slot	$<\delta$			x	x	Coreless
[68]	0–200 k	2-D.1 slot	$<\delta$			x	x	x
[71]	0–800	2-D Full	$<\delta$	x		x	x	
[72]	500–3 k	3-D.3 coils	Some $<\delta$	x	x			Coreless
[84]	0–333	2-D. Half	Fine		x	x	x	
[78]	0–1.4 k	3-D.1 Phase	Fine		x	x	x	nonlinear BH and losses
[66]	0–600	2-D.1 pole		x		x	x	
[70]	10 k–1 M	2-D.1 slot	$<\delta$			x	x	Complex μ. One sheet

[1] Analytical equations are used. [2] Rotor position is taken into account for R and L calculations.

3.1.3. Parasitic Capacitances

As mentioned in Section 2.3, some additional current paths appear at high frequency, due to the existing parasitic capacitances between the different parts of the machine. These paths must be calculated thoroughly as they might have a significant impact on the motor's high-frequency behavior. To analyze these capacitive couplings electrostatic FEM simulations must be conducted [28,52,87].

There are different methods to calculate the capacitances between floating conductors, as explained in [88]. In the electrical machine, those conductors can be the winding conductors as well as the stator and rotor cores, because they behave equally as coupling paths. These are the most used methods [65]:

- Minimum Energy Method: It consist of performing $N(N+1)/2$ simulations, where N is the number of regions to compute. Then, using the electric field value, the stored energy will be calculated. The simplest way to find the self-capacitance coefficients C_{ii}, is to perform N simulations in which all but one conductor are defined with a boundary condition $V_j = 0$ for $j \neq i$. Then, the expression (2) is solved, where W_i is the stored energy and V_i is the applied voltage. To calculate the mutual capacitance between two regions C_{ij}, the boundary conditions $V_j \neq V_i \neq 0$ are defined, where the rest of the regions are set to zero.

$$C_{ii} = 2\frac{W_i}{V_i^2} \quad C_{ij} = C_{ji} = 2\frac{W_{ij} - 0.5(C_{ii}V_i^2 + C_{jj}V_j^2)}{V_iV_j} \tag{2}$$

- Gauss Law method: It consists of performing N simulations in which the conductors are defined with a boundary condition $V_k = 0$ for $k \neq j$. Then, after solving the electric field distribution in each simulation, the expression (3) is applied, where Q_{ij} is the charge of each conductor due to the voltage excitation. $(N+1)/2$ simulations are enough, so that the number of required simulations is notably reduced. Hence, this method can be considered more suitable than the minimum energy method for electrical motors, which normally use coils comprising rather high number of conductors.

$$C_{ij} = 2\frac{Q_{ij}}{V_j} \tag{3}$$

With respect to the model geometry, the capacitances of the active part of the machine can be calculated by 2-D FEM electrostatic simulations, whereas the end-winding capacitances must be calculated by 3-D FEM simulations [73,85]. It must be remarked that the capacitive coupling between the active part of the stator winding and the stator core is significantly bigger than the rest of the capacitive couplings, so that it is the predominant CM current path. Hence, in some cases 2-D FEM simulations are accurate enough to analyze this main CM current path [58]. However, the end winding represents up to 40% of the total winding-to-rotor capacitance and it influences the phase-to-phase capacitance, so it must be considered to obtain accurate results on bearing currents [10,54].

Moreover, the inter-turn and turn-to-stator capacitances result in an NxN symmetric matrix, where N is the number of turns, as shown in (4), where C_{ij} is the capacitance between the ith and the jth turn and the C_{ii} it the ith turn-to-core capacitance [39,42,51,56,62,70]. In [52,55], phase-to-phase capacitance is also defined for multi-layer windings.

$$[C] = \begin{pmatrix} \ddots & -C_{ij} & \cdots \\ \cdots & C_{io} + \sum_{j=1}^{Nc} C_{ij} & \cdots \\ \cdots & -C_{ji} & \ddots \end{pmatrix} \tag{4}$$

In [65] the importance of the mesh between conductors is stated, concluding that at least 2 mesh layers must be defined between conductors to achieve accurate results. The

authors state that the computed matrix shows that the strongest couplings are found for capacitances between neighboring turns and between turns facing the stator core. They stated that the matrix can be simplified neglecting low values of distant conductors, as well as in [51].

In Table 2 the analyzed models are summarized including the purpose of the models and the considered capacitive couplings. It can be seen that the winding-to-stator capacitance is used in all cases, except from the last one, as it analyzes the end-winding influence on the bearing currents, and there, the winding-to-rotor is the most important coupling. Nevertheless, some publications (Winding to ground.) consider the winding-to-ground capacitance instead of the winding-to-stator capacitance, simplifying the models.

It is also remarkable that turn-to-turn capacitances are considered in most cases, especially to analyze transient voltages. Apparently, for CM and DM impedances of electrical machines, the rotor may not have influence, as just some models consider it, while all cases analyzing bearing currents and over-voltages take the rotor into account.

Table 2. FEM Electrostatic comparison.

Case	Experimental Validation	Geometry	Rotor Model	End Winding	Winding Stator	Winding Rotor	Bearing Capacitor	Stator Rotor	Turn Turn
[73]	Bearing Current	3-D.1slot.	x	x	x	x	x		
[85]	CM	2-D/3-D.1/4 Model.	x	x	x	x	x	x	
[54]	CM & DM	2-D.1/8 Model.	x		x	x		x	x
[62]	CM	2-D.1/4 Model.	x		x				(bulk)
[52,86]	Over-voltage	2-D.1/2 Model	x		1				x
[58]	CM & DM	2-D slot	x	2	x	x			x
[61]	Over-voltage	2/3-D	x	x	1				x
[39]	Over-voltage	2-D.1 slot	x		1				x
[51]	CM	2-D.1 slot		2	1				x
[55]	CM & DM	3-D.3 slot		x	x				x
[67]	CM	2-D.1 slot			x				x
[68]	RL	2-D.1 slot		x	1				x
[57]	Capacitance	2-D 1-slot			x				
[65]		2-D 1-slot			x				x
[10]	Bearing Currents	3-D Full	x	x		x	x	x	
[70]	CM & DM	2-D 1 slot			x				x

[1] Winding to ground. [2] Analytical equations are used.

3.2. Analytic Methods

Regarding the analytical methods, some assumptions and simplifications might be made to calculate the resistance, inductance and capacitance values with manageable formulas. Due to these simplifications, generally the analytical calculations are less precise that FEM simulations. However, they require much less computational load than FEM. In this section, some analytical approximations found in the literature are summarized.

3.2.1. Analysis of the Magnetic Core

On the one hand, Eddy current losses rise in the iron core when the frequency increases. In [40], it is assumed that Eddy currents are limited to the skin depth, assuming a uniform current density on it. Then, with the length of the stator, the resistivity and the perimeter of the slot, the resistance of the iron loss due to Eddy currents is obtained to consider it in the circuit.

On the other hand, in [37] the resistance accounting for the core loss at low frequency is considered proportional to the power of the induction machine, and an experimentally estimated damping resistance is added in parallel to the winding inductance to consider the high-frequency iron loss combined with the winding skin and proximity effects. This resistance is added due to the fact that it affects the DM impedance in the first resonance frequency.

No reference to Hysteresis or Excess loss is found, except for the model shown in [47] that uses Bertotti's iron losses estimation. However, the resulting CM and DM currents are not experimentally validated.

Moreover, in [11,48] the common-mode impedance of the stator is calculated. The authors state that when the CM current flows through the stator, a circumferential flux is created in the stator yoke. These currents and flux flow along the iron surface along the skin depth. In the mentioned publications, the magnetic flux in each lamination is the sum of the flux generated by the current flowing through this lamination and the current flowing in the adjacent lamination. Thus, assuming that equal currents flow into each of the N laminations, the core impedance can be calculated in (5) where r_1 and r_2 are the inner and outer diameter of the stator yoke, respectively.

$$Z_c = (1 + j)\frac{N}{3\pi\sigma\delta}\ln\frac{r_2}{r_1} \tag{5}$$

3.2.2. Analysis of Coil Conductors

At high frequencies, the windings are affected by skin and proximity effect as explained in Section 2.1. The first effect can be easily calculated with the well-known Equation (6), where L is the length of the winding, r is the radius of the conductor and δ is the skin depth explained in (1).

$$R_{skin} = \frac{\rho L}{A_{eff}} = \frac{\rho L}{\pi r^2 - \pi(r - \delta)^2} \tag{6}$$

For example, in [40] a single coil of electrical machine is analyzed and the model shows the same trend than the measurements. However, when a group of coils is analyzed, the resistance shoots up due to proximity effect that is not considered in the model, reducing the accuracy of the model.

The proximity effect is not so easy to estimate analytically. The most used method to calculate proximity effect in the literature is [89] and it is applied in transformers. Ferreira proposes a method to calculate the AC resistance of round conductor windings using the exact analytical equations for round conductors, obtaining more accurate results. Nevertheless, some assumptions are still present because they are 1-D flux density models, not considering the effect of leakage flux crossing the slot opening.

In [50] a 2-D analytical model is presented to predict the proximity losses in p.m. machines stator slots, including the effects of slot opening. It is based on the solution of the Laplacian equation in the rectangular coordinate system of the slots in the machine, applying the boundary conditions of the magnetic field intensity. It makes the following assumptions:

- Bundle-level proximity losses are neglected by transposing conductors.
- The slots have a rectangular shape.
- The conductors have a uniform distribution in the slot.

The model is validated with FEM results for single- and double-layer windings, obtaining accurate results up to 1.5 kHz.

In [38] Bessel functions are used to calculate the AC resistance of a shielded multi-conductor, obtaining good results in low frequency but increasing the error up to 12% in high frequency compared to FEM results. This method is also compared with FEM results in [39] for a machine winding obtaining the same error.

In addition, the method proposed in [37] uses the Institute of Electrical and Electronics Engineers (IEEE) standard Induction Machine (IM) circuit [90] obtaining the parameters from the manufacturer data sheet. Then, some add-ons are proposed to account for the high-frequency effects. The inductance of the first turns of the winding is added, as it influences the high-frequency anti-resonance point. A stator turn-to-turn damping resistance is defined also to account for the skin and proximity effect of the wire. There is not perfect

matching of DM impedance because the stator leakage inductance skin effect is not taken into account.

Summarizing the relevant cases obtained with analytic methods in Table 3, it can be seen that the accuracy is lower than in FEM methods, and their frequency range is smaller. One method is only found to obtain proximity effect losses in electric machines directly [50], as the dumping resistance inserted in [37] accounts for skin and proximity effects in the winding and high-frequency iron losses in the machine.

Table 3. Analytic simulation comparison.

Case	Frequency Range	Iron Core	Proximity Effect	Capacitive Coupling to Ground	Validation
[40]	0–80 k	Eddy Currents		Parallel plates	Single coil
[37]	0–1 M	Dumping resistance	Dumping resistance	Bulk winding	DM CM (Not adjusted resonances)
[47]	0–200 k	Bertotti	FEM	Lumped C network	
[50]	0–1.5 k		Laplacian Equation		Joule Losses in PMSM (Error < 10%)
[38]	0–10 M	(Shielded cable)	Bessel function		R & X with FEM (Error ≈ 12%)

3.2.3. Parasitic Capacitances

When the working frequency increases, the impedance of parasitic capacitances decreases, leading to new current flow paths inside the motor which affect its DM and CM impedances. The analytical calculation of capacitances is spread out in the literature.

- **Stator-Winding-to-Rotor Capacitance:** In [41,43] each slot is considered to be a plate capacitor. This capacitor consists of the airgap and the height of the slot opening with the permittivity of the air and the slot wedge and the upper slot insulation with the insulation material relative permittivity. This approach shows an approximate error of 15 % due to geometrical approximations.

  The method of image charges for the solution of Laplace equation is used by Stockbrügger and Ponick to calculate winding-to-rotor capacitance. This method replaces the elements in the geometry with imaginary electric charges, replicating the boundary conditions of the problem. It uses line charges for the slot portion and ring charges for the end-winding portion. The results show small deviations with FEM results enabling the prediction of bearing voltage.

  Moreover, the end-winding contribution to the winding-to-rotor capacitance must be calculated. In [58], authors state that the end windings typically have a rectangular structure. Thus, the capacitance is estimated using the equation for a cylindrical capacitor (7), where ε_r is the relative permittivity, ε_0 is the permittivity of the vacuum, l_{ew} is the length of the end winding and d_r and d_{air} are the rotor diameter and the airgap, respectively. The obtained result is added to the rest of the winding-to-rotor capacitance, validating it with FEM results, with some deviations.

$$C_{wr,ew} = \frac{2\pi\varepsilon_r\varepsilon_0 l_{ew}}{3} \ln\left(\frac{d_r + 2d_{air}}{d_r}\right) \tag{7}$$

- **Rotor-to-Stator Capacitance:** The stator and rotor are considered to be cylindrical capacitors. To account for the influence of the slot openings, a coefficient is added similar to the one used to for the reduction of the airgap flux density in magneto-static calculations, called Carter´s coefficient. The calculated values show a difference of 15% from measurements, but the author states that the values are in the safe side, as the bearing currents are overestimated by this method [41].

- **Bearing Capacitance:** The bearing acts as a capacitor if it rotates at a sufficient speed for an electrically insulating lubricating film to build up and if the voltage applied is lower than the electrical break-down threshold. The value is calculated taking into account the minimum thickness of the lubrication film and the Hertzian contact area [41]. The proposed model is validated with bearing voltage measurements.

- **Turn-to-turn Capacitance:** In [42], an analytical model of a winding is presented to predict the turn-to-turn capacitance. The capacitance for nonadjacent turns is not taken into account as it is assumed that the flux lines are only directed towards the next immediate conductor. The turn-to-turn capacitance is the series of the airgap and coating capacitances. In other words, the global accuracy of the analytical results compared to FEM results is questionable looking the relative error. However, results converge to the same order of magnitude.

  Moreover, in [46] the turn-to-turn capacitance for rectangular cross-section windings is calculated assuming they are two plate capacitors, but the analytic values differ from FEM results. Moreover, in [45] it is stated that depending on the real configuration of the winding, different analytical methods must be used, otherwise the result can have a 400% of deviation. One of the methods can be used when round wires are largely distanced and in single layer windings, whereas the other method can be used when the distance between wires is small compared to the diameter, as it considers that the conductors are touching each other. It is important to know the details of the electrical machine design before applying any calculation method [91].

- **Winding-to-Stator Capacitance:** In [43], the winding turns are treated as a unique winding region and the capacitance between the stator winding and stator core is considered a plate capacitance. This simplification is not acceptable looking at the results.

  On the contrary, in [42] the iron core surface is considered to be a perfect equipotential, so the electric field lines are orthogonal to the surface of the core. In that case, turn-to-core electric field lines go through half of the path compared to the turn-to-turn lines. The turn-to-stator capacitance is estimated as the double of turn-to-turn Capacitance [42,92]. However, based on FEM results, turn-to-stator capacitance must be 2.4–3 times the turn-to-turn Capacitance.

Finally, in Table 4 different publications are compared regarding the capacitance calculation on electric machines, including the method or main geometrical simplification and the approximate error compared to measurements. It can be seen that the accuracy is limited in most cases, but may be enough for come approximations, as mentioned in those publications. It is important to know the geometry of the machine before choosing a calculation method.

Table 4. Analytic Capacitance comparison.

Case	Winding Stator	Winding Rotor	Stator Rotor	Turn Turn
[41]		Plate capacitors ($\approx$15%)	Cylindrical caps ($\approx$15%)	
[43]	Plate capacitors ($\approx$80%)	Plate capacitors ($\approx$30%)	Cylindrical caps ($\approx$20%)	
[79]		Image charges (4–10%)		
[58]		Cylindrical capacitors ($\approx$30%)		
[42]	$2C_{tt}(\approx$50%)			Conductors($\approx$32%)
[45]				For single layer ($\approx$15%)
[46]				Plate capacitors($\approx$16%)

3.3. Measurement-Based Methods

The last approach to model an electric motor for HF analysis is measuring both DM and CM impedance and getting the circuit parameters from those measures. It is a very used approach, but it is not practical during the design process, as a prototype is needed. When obtaining impedance vs. frequency curves, two different connection layouts are usually used [12,13,15–17,20–24,26–29,31–33,35,36]. In Figure 6a CM impedance measuring layout is shown, while in Figure 6b DM impedance is measured.
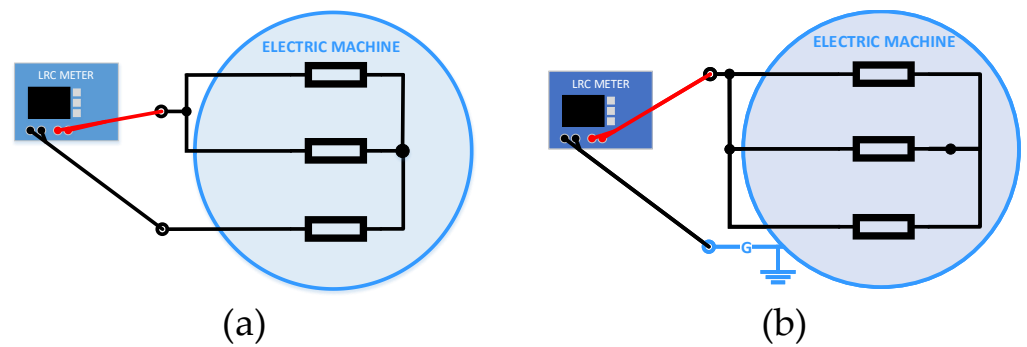
Figure 6. Impedance measurement connection layout. (**a**) CM; (**b**) DM.

Additionally, in [21,22,26,28], it is stated that even if IPMSM have been widely treated as IM for the simulation of EMI, the characteristic impedance is different as DM impedance varies with the rotor position due to the variation of reluctance, as shown in Figure 7.
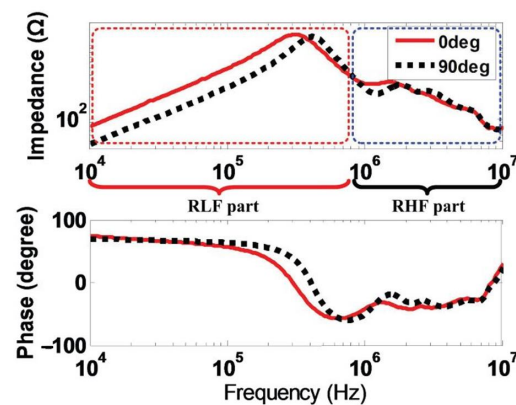

Figure 7. Differential-mode Impedance [28].

Thus, [22] introduces a new measurement consisting of measuring the impedance of two phases in series. Then, the equivalent inductances are calculated for different rotor positions. Moreover, in [12,17] some additional measures are needed to complete the model parameters.

Alternatively, [30] analyzes the ground current of an induction machine and measures the CM impedance as shown in Figure 6a and the impedance between the three-phase terminals and the motor neutral with a floating ground terminal.

The procedure for calculating the LPM parameters is dependent of the proposed model. Most models have fixed LRC sections [12,13,15,17,19,20,24,29–33,35,36], whereas some of them have as many LRC sections as the number of resonance points of the impedance curve [26–28].

Most authors give a physical meaning to the RLC values, others relate the RLC value to a point or region in the impedance curve [17,22,24,28] or even use data fitting methods where the resistance value can be even negative [15,16,93]. In [23], some initial parameters of the model are calculated analytically from the impedance curve, and a minimization algorithm is proposed for the rest of the parameters, restricting the values to real positive ones.

After this main classification of the methods is done, some relevant details about the methods are commented.

In Figure 8 the DM impedance measurement and an equivalent circuit are shown. Usually the resonances around the EMI analysis range (150 kHz–30 MHz) are only considered and to avoid numerical difficulties, each selected pair of peaking and dipping frequencies should be sufficiently apart from each other. To simplify the characterization, it is assumed that the inductance in each stage of the circuit of Figure 8a is much smaller than

the next stage to its right. The authors in [27] note that this is just an assumption imposed on the behavioral model and does not have implications in the machine behavior.
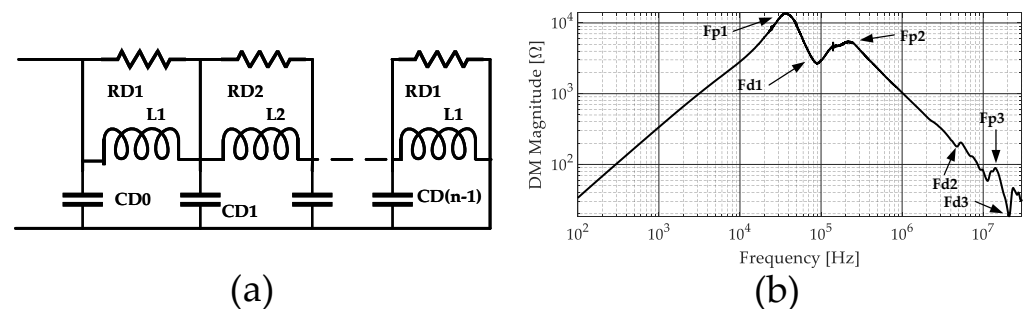

Figure 8. Measurement-based modeling of an IM. (**a**) Typical single-phase equivalence for DM impedance; (**b**) DM impedance.

DM parameters are determined from the peaks and dips identified in Figure 8b, not with any physical meaning. After following the same procedure with the CM impedance, a three-phase equivalent circuit is composed, integrating the motor in the electric drive model and validating it up to 10 MHz.

Furthermore, in [22,26,28], the model is divided in two sub-circuits. One referring to the low-frequency range, where the rotor position influences the RL values that are obtained with FEM, and a high-frequency range circuit, where the values just depend on frequency and not position. This model is validated with measurements, obtaining good accuracy below 3 MHz.

In the case of [12], also five tests are done to extract the parameters, but the rotor is taken into account, so rotor-to-stator capacitance is also extracted. The main drawback of this method is the need to electrically isolate the rotor from the frame to measure rotor-to-stator capacitance. This method and the proposed model are validated both for EMI and shaft voltage analysis. [23] uses a Lumped equivalent circuit from a different point of view. The identification is performed for a set of measured complex CM and DM impedances from 11 electrical machines of the same type. Initial parameters are determined through approximations from the measured data and the rest are obtained by a minimization algorithm, resulting in a model matching the measured results up to 30 MHz.

In [20] it is noted that the iron loss resistance is responsible for the damping of the first resonance in DM, so it obtains the value of R_e from the impedance value at that point. Then, an extension is made to the model, and it is shown that better results are obtained if R_e is defined as a frequency-dependent resistance that reproduces the skin effect of the iron core.

Furthermore, in [24] a combined method is proposed to obtain the model parameters with CM and DM measurement together with FEM simulations. The model includes Eddy current loss, the inter-turn effects of the winding and the leakage inductance effect of the first few turns of the winding. However, in the low-frequency range, the DM impedance is affected by the stator magnetization inductance and the core losses resistance. Here, the unknown parameters are more than the equations that we can derive from DM impedance characteristics. Therefore, 3-D FEM is used to calculate the core losses.

Finally, in [94] a model of a PMSM proposed in [33] is integrated into the whole drive with the inverter and the power cable that are also modeled. The inverter, power cable and the PMSM are validated individually, and finally, the whole model is validated, obtaining a rather good accuracy with the measured spectrum. However, further validation is required from 10 to 30 MHz due to the electromagnetic noise induced in the voltage probes and current transducers.

4. Modeling of Electrical Machines in High-Frequency

In the previous section, three different analysis tools are described for high-frequency electrical machine analysis. From that analysis, some electrical parameters are obtained (L, R, C), to introduce them in different models. In this section, the main models are classified based on their topology, parameter extraction methods and their main characteristics.

Concerning their complexity or size, the models can be classified into two categories. Distributed Parameter Models (DPM) and Lumped Parameter Models (LPM). DPM tend to be more accurate, but they may not be integrated with other system components, as they need intensive computation [39,51,52,56,58,61,62,86].

By contrast, LPM is more practical, as it can be introduced in a complete electrical drive model, and its parameters can be obtained from simple impedance measurements [13,17,20–24,26,27,31,32,35,37,54,55,73]. Some authors develop high accuracy DPM models and simplify it to LPM with matrix reduction methods [52] or by grouping the RL parameters [58]. A review of the different models is made in Table 5.

Table 5. Model Comparison.

Model	Frequency Range	Model Type	Parameter Extraction	Inter-Turn Effects	Bearing Model	Rotor Model	Integration in Drive	Simulation Domain	Iron Loss
[32]	1 k–13 M		Measured	x	x		x	Freq & Time	Implicit
[17]	10 k–10 M		Measured	x	x		x	Freq & Time	Implicit
[20]	10 k–10 M		Measured				x	Freq & Time	R Parallel
[23]	10 k–10 M		Measured	x				Frequency	Implicit
[31]	100 k–500 M		Measured					Frequency	Implicit
[12]	10 k–10 M		Measured	x		x	x	Freq & Time	Implicit
[13]	100–100 M		Measured	x				Freq & Time	R
[21]	150 k–10 M	LPM	Measured	x		x [1]	x	Freq & Time	R
[33]	100–30 M	Fixed	Measured	x		x	x	Freq & Time	R
[24]	100–10 M	Segments	Measured [2]	x				Frequency	R|L|RC
[15]	100 k–100 M		Measured					Freq & Time	Implicit
[35]	10 k–1 M		Measured	x				Freq & Time	Implicit
[36]	100–10 M		Measured	x				Freq & Time	R Parallel
[37]	10–10 M		Analytic	x	x	x	x	Freq & Time	R Parallel
[73]	30–5M		FEM [3]		x	x		Time	RL
[54]	100–100 M		FEM	x	x	x	x	Freq & Time	Implicit
[27]	1 k–10 M	f(F)	Measured				x	Freq & Time	Implicit
[22]	10 k–3 M	Segments	Measured [2]			x [1]		Freq & Time	Implicit
[62]	20–4 M		FEM [3]	x				Frequency	Implicit
[86]	10 k		FEM	x		x	x	Time	Implicit
[58]	100–1 M		FEM [3]	x		x	x	Frequency	R Parallel
[61]	0–100 k	DPM	FEM	x		x		Time	Implicit
[39]	10–10 M		FEM	x				Freq & Time	Implicit
[51]	1 k–10 M		FEM	x				Freq & Time	Implicit
[55]	10 k–20 M		FEM	x				Frequency	Implicit
[70]	10 k–1 M		FEM	x				Frequency	Implicit

[1] The rotor position is also considered. [2] FEM is used for some parameters. [3] Analytical equations are used for some parameters.

With respect to the simulation domain, some models are working in the frequency domain, for example, to obtain the CM and DM impedance versus frequency. However, to simulate the over-voltages and currents, the time domain is needed. In this domain, the frequency dependency of the parameters is usually considered using lumped parameter circuits, as varying the value for each frequency may not be practical. Two main methods are exposed here.

In [58] four parallel RL branches are used to reproduce skin and proximity effects in the resistance and inductance values, where each branch represents a frequency range. The resistance of the first branch, representing the low-frequency range is received directly from FEM values whereas the following branch resistances are calculated by a frequency-

dependent formula and the decrease of the inductance with the frequency is represented by two empirical factors obtained from [95]. The resultant impedance is shown in Figure 9.
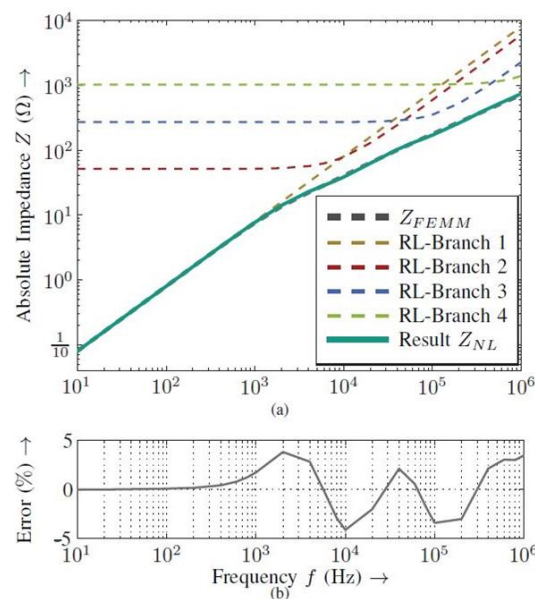

Figure 9. Impedance result of RL-branch compared to FEM in [58]. (**a**) Impedance (**b**) Error.

Something similar is used in [22,26,28] for taking into account the resistance and inductance variation with frequency. They use Foster's network, adjusting their values with data fitting procedures. The models are validated obtaining accurate results.

Even if all models are based on LCR circuits, they refer to different parts of the machine and include different high-frequency phenomena:

- **Inter-turn effects:** To make an accurate model in high frequency, the influence between conductors must be modeled. Most FEM-based models consider these effects in the analysis, and in measurement-based methods, this is implicitly included.

- **Bearing:** Just a few models include the bearing in the model, as their capacitance is important when simulating bearing currents, but in the rest of the models they are neglected or calculated analytically [41] or empirically [53,54]. Bearing capacitance can be neglected when using plastic bearings or when the machine is in stand-still as mentioned by [43,58]. In [37] the rotor, the shaft and the bearing models are included, so it is very useful to analyze the motor's behavior over a wide range of frequencies and it can be also suitable for the study of bearing currents and CM shaft voltage both in time and frequency domain.

- **Rotor:** As C_{wr} & C_{sr} are 10^3 times smaller than C_{ws}, the rotor does not affect DM impedance in high frequency, but when analyzing CM current paths, stator-to-rotor capacitance is essential, so modeling the rotor is needed [37,58]. A reduction of 16.4% of the maximum over-voltage is found in the case of the turn-to-ground voltage when including the rotor, so it is fundamental for insulation design too [61]. Additionally, in [21] a conventional dq Interior Permanent Motor model is improved by adding the ground capacitance, the iron loss resistance and a ground resistance. In this way, the values RL remain constant, regardless of the rotor position, like in the machine models used for control purposes.

- **Iron Loss:** Considering the explained in Section 2.2, Eddy currents are essential at high frequency. Some models include a loss resistance in parallel with the winding impedance, whereas others do not refer any specific parameter in the electrical circuit to account the losses, being implicit in the circuit values. In [24], an R in parallel with L and a RC is proposed to account for the Eddy current effect in the iron in the mid-frequency range.

As an example, a distributed parameter turn-by-turn model is proposed in [62]. The RLC-parameters are derived from 2-D FEM simulations and analytical expressions. It takes into account turn-to-turn capacitance and the capacitance of the iron core. An interesting point of this method is the fact that the circuit is defined in a matrix way, so the calculation of the CM impedance is really fast. It matches the measures until 4 MHz. A similar approach is used to model the resonances and the frequency response in transformer windings using inductance and capacitance matrices in [96,97].

It is remarkable that [31] proposes a high-frequency model in the range of 100 kHz–500 MHz for PMSM in electric vehicles, being able to model the irradiated EMI frequency spectrum including Delta connected stators, but the accuracy of the impedance value at resonant frequencies is limited.

5. Influence of Design Parameters on EMC

Once the machine EMI behavior is analyzed by developing different models shown in the previous section, the influence of different aspects must be evaluated using those models. Different factors may affect the EMC behavior, such as design parameters, manufacturing materials, and fabrication processes and tolerances. To go to the detail of the design parameters and tolerances, normally FEM analysis is used as the main option.

5.1. Power Rating

Even if [20] mentions that construction materials and tolerances have a non-predictable influence on the model parameters, it states that winding-to-stator capacitance increases with the power rating due to the thicker wires used in higher power machines, increasing the turn-to-stator area. It is also mentioned that stray inductance decreases when the power rating increases. However, the power rating is not a variable that can be used to optimize the EMC behavior of the machine as it is set by the application, being one of the principal requirements.

5.2. Grounding Points

With respect to CM current flowing path, in [98] it is mentioned that the number of grounding points and their position in the machine frame can change the HF current flowing paths. The HF currents always go to the grounding point thorough the surface of metallic parts, but the current will flow divided in different paths depending on the path impedance.

5.3. Winding Configuration

It is found that the impedance of a series connected winding machine is four times higher than in a parallel connection one since a winding inductance varies as N^2. Additionally, the first resonance frequency of a parallel machine connection is almost double the resonance frequency of a series winding connection machine [36,37].

Furthermore, the star and delta winding connections are also analyzed in the literature. In [32] it is shown that CM impedance of both connections is mainly capacitive, but the resonance frequency is 6 times higher in the delta connected machine. The impedance below and above the resonance points is equal as the CM paths in these frequency ranges are equal for both connections. Equally, even the shape of the DM impedances of both winding connections is equal, the amplitude of the star connection is higher than the amplitude of the delta connection in the whole frequency range. The authors mention that this difference is due to the DM path. For the delta connection, the DM path is composed of approximately two parallel windings, whereas for the star connection this path is made of one winding in series with two parallel-connected ones. In [36], the connections of the machine are also analyzed and a model valid for series, parallel, star and delta connections is proposed.

In [37], where it measures a 5 hp induction motor, it mentions that a delta connection winding has twice the stator winding-to-ground effective capacitance compared to a star connection.

Regarding the winding topology, in [14] circumferential (CW) and toroidal winding (TW) topology are analyzed. The first one is the typical concentrated winding in electrical machines, whereas in the second, the winding forms a kind of toroid, reducing the end windings. It is concluded that even TW may be better for thermal management and higher power density, they increase winding-to-ground capacitance, increasing the CM current by about 20 dB.

5.4. Conductor Placement and Impregnation

The placement of the conductors in the slot is very important to model the CM current and voltage, as the skin and proximity effects have a great impact on the voltage distribution of the windings and the insulation stress of the conductors [39,99]. The further the winding conductors are from the rotor, the lower winding-to-rotor capacitance will be, and the lower the bearing currents will be [53].

Concerning to the orientation of the conductors with respect to the leakage flux lines, in [66,99] it is found that the lowest copper losses are generated when the strands are aligned in the direction of the leakage flux lines. Then, a bit higher losses occur if strands are arranged in compact bundles and significantly higher losses occur when the strands are aligned in perpendicular to the flux lines. The voltage level also influences the copper loss. For the same power, the lower is the voltage, the higher is the AC loss due to the increased cross-section of the conductor to carry higher currents.

Moreover, it is found that lower capacitance is obtained if the conductors are located near the middle of the slot instead of near the tooth edge, as shown in Figure 10. Equally, the slot shape may also affect winding-to-rotor capacitance and the shaft voltage, as it directly affects to the conductor position [12,57].

Moreover, it is found that a small quantity of impregnation decreases the stray capacitance, but this may affect to the thermal and mechanical performance as shown in Figure 10, so an equilibrium must be found [57]. Sarrio et al. make an analysis to see the influence of the insulation in the whole capacitance matrix of a slot. The capacitive coupling is proportional to the amount of dielectric material in the slot.
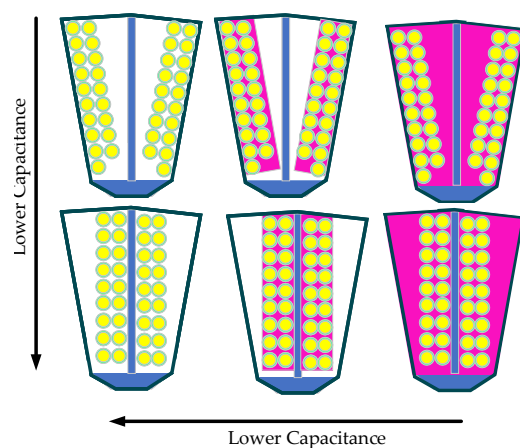

Figure 10. Winding position and impregnation.

Taking this to a more practical approach, in [44] an optimization algorithm is proposed to improve the EMC behavior of DC machines modifying the winding insulation thickness, material and the placement of the conductors, obtaining close results. This must be the objective when designing electrical motors for EMC optimization, but a broader analysis must be made to consider all influencing parameters.

5.5. Additional Actions

After the basic machine design, some additional actions may be taken to decrease EMI in electrical machines once they are manufactured. For instance, in [53] insertion of additional grounded electrodes into the slot wedge leads to reduce the winding-to-rotor capacitance, minimizing the non-circulating bearing currents.

Moreover, [100] proposes reducing the absolute value of the magnetic flux leakage by a two-layer shielding of the machine, intending to reduce the induced voltage in the surrounding electrical loop. However, as shielding the whole machine may be too expensive and bulky, in [10] shielding of the end windings is proposed to reduce the winding-to-rotor capacitance and the bearing currents, as the end winding represents less than the 1% of winding-to-stator capacitance but up to 40% of the total winding-to-rotor capacitance and it influences the phase-to-phase capacitance [10,54]. Different shielding methods are proposed, showing different C_{wr} reductions, and a good achievement is made for bearing health and life expectancy. Even if the mayor reduction would be achieved with the solid shielding, as it increases the iron losses, the Faraday's cage shielding could be a better option.

Additionally, there are some external factors beyond the machine that can affect EMI behavior, such as inverter modulation pattern and frequency, DC bus voltage, but there are out of the scope of this work [1,12].

Although the machine operating point or its torque angle may also affect DM EMI level, this cannot be used as an EMI improvement way, because it would reduce the working range of the machine [26]. Something similar happens with the influence of airgap size on the stator-to-rotor capacitance, as it affects to the EMI behavior but also to the machine performance [12].

Finally, as an introduction to the future work, in [101] a new systematic method is proposed to quantify the influence of tolerances on PMSM performance to identify possible non-compliant-dimensional variables and material characteristics, based on the results of the open-circuit and short-circuit procedures of IEEE Std 1812. Design of Experiments (DOE) is used to analyze the influence of each analyzed parameter. In this case, short-circuit current, torque ripple, open-circuit voltage, and core losses are analyzed as output variables, but it may be useful when analyzing the influence of tolerances and design parameters on high-frequency behavior.

Summarizing, an overview of the different studied design parameters influencing the high-frequency behavior of the machine is shown in Table 6.

Table 6. Design parameter influence review.

Parameter	Impact	Optimum
Parallel Circuits	First resonance frequency	$f_{rSeries} = \frac{1}{2} f_{rParallel}$
Y-Δ Connection	First resonance frequency in CM Impedance DM Impedance Amplitude	(Δ higher than Y) (Y higher than Δ)
Conductor placement	Cwr & insulation stress Bearing & CM Currents Shaft Voltage Copper Losses	Furthest from rotor Middle of the slot Strands aligned with flux lines
Winding Topology	Winding-to-ground capacitance	Circumferential winding
Impregnation level of conductors	Stray Capacitance	Low (affects thermal)
Slot Shape	C_{wr}, Shaft voltage	-
Electrodes in slot wedge	Cwr & insulation stress Bearing & CM Currents Shaft Voltage	High diameter Nearest from rotor >1 electrodes together
Airgap size	C_{rs}	Minimum
Shielding	Induced voltage	Depends on frequency
End-winding shielding	C_{wr}	Faraday's cage *

* An equilibrium must be made between the shielding structural complexity and the C_{wr} desired reduction.

6. Conclusions

In this paper, a thorough review of high-frequency analysis and modeling tools for electrical machines is performed. In addition, the main design parameters that affect to the high-frequency behavior of electrical machines are identified. In this section, the main conclusions are outlined as the results of this review.

First, it should be mentioned that generally the models presented in the literature are not demonstrated to be accurate in the overall range of frequencies covered by EMC standards (from 0 Hz to 30 MHz). All proposals found in the literature show rather good accuracy up to 10 MHz, but not in the range of 10 MHz and 30 MHz. It would be convenient to extend the precision range up to 30 MHz. In addition, the technological development in electronic switching devices are leading to higher working frequencies. Due to the fact that higher precision range above 30 MHz is recommendable because the standard levels might increase as the working frequency of devices increases.

Next, the main conclusions related to every topic reviewed in this paper are summarized.

6.1. High-Frequency Phenomena

In the winding, the skin and proximity effects increase with frequency, affecting both the resistance and the inductance values of the coils. To model those effects correctly, a detailed geometry of the stator slot must be considered, and the location of the conductors inside the slot must be also roughly described. The skin effect depends on the wire diameter and frequency, so it can be eliminated using conductors smaller than the skin depth in parallel strands. However, a high number of strands is counterproductive after a point due to the proximity effect, being also more difficult to manufacture. Litz wires are used to reduce skin and proximity effects, with an especial transposition to reduce the proximity effect, but above a frequency, the proximity effect is not softened.

Regarding the capacitance couplings, the properties of dielectric insulation materials must be precisely known. Otherwise, the computation of the capacitances might differ from real values. It is remarkable than when manufacturing the electric machine, some conductors may vary their position from the theoretical one, making the capacitance calculation differ from the measures too.

Moreover, the end-winding must be also considered, including the skin and proximity effects in that region. Concerning the capacitive coupling, even if the end winding represents less than the 1% of winding-to-stator capacitance, it is up to 40% of the total winding-to-rotor capacitance and it influences the phase-to-phase capacitance, so it must be taken into consideration.

With respect to the magnetic core, Eddy currents are significant in high frequency. Not only due to the iron losses they create, but also due to the shielding effect they produce. Due to this shielding effect, the magnetic flux is pushed out from the magnetic core, decreasing the effective ferromagnetic material area and leading to a decrease in the value of the winding inductance. The frequency when the shielding effect starts depends on the thickness of the sheet and its resistivity. The lamination of the stator prevents the flux being totally pushed out of the core, leading to a higher winding inductance compared to a bulk stator. The effect of lamination also leads to a higher resistance of the winding compared to a bulk core because the surface area where Eddy currents flow is larger and the proximity effect between sheets increases the Eddy currents in the core.

6.2. Analysis Tools

Regarding the FEM analysis, the detailed geometry of an electric machine can be accurately modeled obtaining precise resistance and inductance values, taking into account the skin and proximity effects, as well as eddy current losses in the stator and the capacitive couplings. The mesh of the geometry is essential to obtain accurate results in FEM. When working in high frequency, the skin depth of the materials must be finely meshed, both in the conductors to consider skin and proximity effects, and in the core, as the Eddy currents flow along the skin depth of the iron sheets. Thus, the mesh size must be thinner than the

skin depth. However, this meshing requirement leads to a higher time consumption and computational load. Thus, an equilibrium must be found between the model complexity and the accuracy. For the active length of the machine, 2-D simulations are usually used, even if the resistivity of the sheets must be calibrated to take into account the lamination effects, usually using 3-D models. It must be remarked that not all iron sheets comprising the magnetic core can be modeled in 3-D with a mesh size thinner than the skin depth, otherwise, the model will take ages to solve. Commonly, 2 or 3 sheets are simulated and the results are extrapolated to the whole length. Even if the 3-D FEM is the most complete simulation tool, it is the most computationally demanding too, so it is usually only used for the end-winding calculation, as it is the only way to calculate it accurately. Once a 3-D FEM simulation is done, some authors propose different coefficients to take into account this end winding, by using just 2-D FEM for successive simulations. With respect to the capacitance calculation in electrostatic FEM, the same applied to magnetic calculation is applied, needing 3-D models for the end winding, at least for the winding-to-rotor capacitance calculation, where it has a big impact. In this case, a 2 mesh layer must be defined between the conductors for turn-to-turn capacitance accuracy. Gauss Law method is recommended for the calculation of the capacitance matrix, as it requires fewer simulations.

In the case of analytical tools, commonly they require less computation time, as some assumptions and simplifications are considered for each specific case. The skin effect can be easily calculated analytically reducing the effective cross-section area of the conductors. Nonetheless, the computation of the proximity effect is not so simple due to the non-uniform distribution of the magnetic field in the slot. Bessel functions have been used to calculate the AC resistance of the winding, leading to 12% errors at 50 MHz. An analytical method is found to calculate the Joule losses taking into account the proximity losses, but an uniform conductor distribution is assumed in a rectangular slot, so it may not be applicable to all cases, and it is only tested until 1.5 kHz so it may need further development for using it in EMC analysis of electric machines. With respect to the capacitance values, geometric simplifications are done to simplify the calculations to plate capacitors in the case of the winding-to-rotor capacitance or cylindrical ones for the stator-to-rotor capacitance, and even if they converge to the same order of magnitude, they are not accurate enough. A novel approach is proposed for the determination of the winding-to-rotor capacitance using the method of image charges, validating the results with FEM. In the turn-to-turn capacitance, some methods can reach acceptable results. For the turn-to-turn capacitance calculations, the method must be chosen depending on the specific disposition of the winding, otherwise, large errors can appear.

Concerning measurement-based tools, rather good accuracy can be reached by adjusting the model behavior in the whole frequency range. Nevertheless, it is important to underline that this approach is not suitable for the design stage of the motor, as the prototype must be already built to perform the experimental impedance measurements, and then obtain the parameter values by curve fitting. For example, this approach should be suitable for analyzing the behavior of the overall electric drive in simulation, considering the high-frequency models of the motor, the inverter and the EMC filter, but not for predicting the behavior of the electrical machine during the design process. Inside the measured-based tools, there are two different ways of obtaining the electrical circuit model, by looking for the physical meaning of each parameter and relating it to the impedance curve, or just by parameter fitting procedures, obtaining even negative values. This model can obtain excellent accuracy in the whole frequency range.

All in all, FEM tools are recommended for a detailed high-frequency analysis of electrical machines during the design stage. They take into account all high-frequency phenomena and obtain very accurate results provided that the geometry and mesh are properly defined.

6.3. Modeling

The high-frequency models of electrical machines can be classified based on their topology, parameter extraction methods and their main characteristics as well as on their working domain. Distributed parameter models tend to be more accurate, but they are difficult to integrate in the whole electric drive due to the intensive computation required. Lumped parameter models are more used as they are more practical. The values of the LPM are usually calculated from measurements, but there are some DPM obtained from FEM values that are converted to LPM with matrix reduction techniques.

With respect to the simulation domain, some models are working in the frequency domain, for example, to obtain the CM and DM impedance versus frequency. However, to simulate the over-voltages and currents, the time domain is needed. In this domain, the frequency dependency of the parameters is usually considered using RL parallel branches or foster networks, as varying the value for each frequency may not be practical. If frequency-dependent values are obtained from FEM, the equivalent RL branches can be obtained using data fitting methods.

Finally, depending on the objective of the simulation, the developed model may highlight or neglect some parts of the machine. On the basis, all models are RLC circuits, with different number of segments and different physical meanings, but in origin, all refer to winding self and mutual inductances, resistance and parasitic coupling capacitances. The inter-turn effects in the winding are essential to obtain accurate results, whereas the bearing capacitance is just included when the bearing currents are analyzed. The iron losses produced by Eddy currents in the stator sometimes are included as a resistor in parallel with the winding, whereas other times the losses are just implicit in the circuit values.

Concerning the rotor, its influence may be only significant when analyzing bearing currents, shaft voltages, or terminal over-voltage. The rotor position is also important in the low-frequency range for salient pole permanent magnet machines as the inductance changes with the rotor position. Hence, if a full frequency range (0 Hz–30 MHz) model is required, the rotor should be considered.

6.4. Influence of Design Parameters

Different factors may affect the EMC behavior of electrical machines, such as design parameters, manufacturing materials, and fabrication processes and tolerances. To go into detail on the design parameters and tolerances, normally FEM analysis is used as the main option.

Concerning the winding connection, the first resonance frequency of the CM impedance is higher for a Delta connection, whereas the DM amplitude is higher for a star connection. The presence of parallel circuits increases the first resonance frequency to double.

In relation to the conductor placement in the slot, their optimum position is furthest from the rotor, just in the middle of the slot. In this way, winding-to-rotor capacitance is reduced, decreasing the insulation stress, the CM current and the shaft voltage. The capacitances also depend on the impregnation amount. The less the impregnation quantity is, the lower the capacitance is. Moreover, if the strands are aligned with the flux lines, the copper losses will decrease.

Additionally, electrodes can be inserted in the slot wedge to reduce bearing current and the shaft voltage, and shields can be added to the end windings or to the whole machine to reduce the winding-to-rotor capacitance, but these solutions might increase the cost and weight of the machine.

The analysis found in the literature is mainly focused on reducing bearing currents and insulation stress, so a broader approach may be needed to make an EMI strategy-based design for electric machines.

6.5. Future Trends

All in all, a new design methodology should be developed for electrical machines, including electromagnetic, thermal, and EMC optimizing procedures. In this way, the electric drives would be more competitive at the design stage, reducing reworks to comply with EMC requirements. To do so, the explained analysis tools may be combined taking into account the mentioned considerations. First FEM tools must be used to obtain accurate results, then the existing analytical tools may be completed or improved to make faster calculations. Moreover, a more extensive analysis must be performed to identify and quantify the influence of the different design parameters on the EMC behavior of the electrical machines, as this is the key for the optimization.

The present review is the basis to continue developing high-frequency models of electric machines. It gives an overview of the different physical effects that occur at high frequency, together with the different tools to model this phenomenon. The influence of different design parameters in the machine behavior is also summarized. This review is considered to be a necessary contribution to establish a solid foundation for future work in the EMC optimization in electrical machines.

Author Contributions: Conceptualization: Y.M., G.A. and A.E. Investigation: Y.M., G.A., A.E. and B.A. Formal Analysis: Y.M., G.A., A.E. and B.A. Project administration: G.A. and A.U. Supervision: G.A. and A.E. Writing—original draft: Y.M.; Writing—review and editing: Y.M., G.A., A.E., B.A. and A.U. All authors have read and agreed to the published version of the manuscript.

Institutional Review Board Statement: Not applicable.

Informed Consent Statement: Not applicable.

Data Availability Statement: Not applicable.

Conflicts of Interest: The authors declare no conflict of interest.

Abbreviations

The following abbreviations are used in this manuscript:

CISPR	International Special Committee on Radio Interference
CM	Common-Mode
DM	Differential-Mode
DOE	Design of Experiments
DPM	Distributed parameter circuit
EMC	Electromagnetic Compatibility
EMI	Electromagnetic Interference
FEM	Finite Element Methods
HF	High-Frequency
IEEE	Institute of Electrical and Electronics Engineers
IM	Induction Machine
LPM	Lumped parameter circuit
PMSM	Permanent Magnet Synchronous Machine
PWM	Pulse width modulation

References

1. Zhang, J.; Shen, M.; Zhao, X. *Study on the Effect of Inverter Modulation Methods and Operating Condition on Common Mode EMI for Motor Drive System*; SAE Technical Papers; SAE International: Warrendale, PA, USA, 2017. [CrossRef]
2. Shen, Z.; Jiang, D.; Zou, T.; Qu, R. Dual-Segment Three-Phase PMSM with Dual Inverters for Leakage Current and Common-Mode EMI Reduction. *IEEE Trans. Power Electron.* **2019**, *34*, 5606–5619. [CrossRef]
3. Mazurck, P.; Michalski, A.; Swiatck, H.; Mazzetti, C.; Flisowski, Z. Hazard for insulation and relevant emc problems due to voltages in circuits of motor supply by pwm converters. In Proceedings of the 2003 IEEE Bologna Power Tech Conference Proceedings, Bologna, Italy, 23–26 June 2003; Volume 2, pp. 728–732. [CrossRef]

4. Ferreira, F.J.; Trovão, J.P.; De Almeida, A.T. Motor bearings and insulation system condition diagnosis by means of common-mode currents and shaft-ground voltage correlation. In Proceedings of the 2008 International Conference on Electrical Machines, ICEM'08, Vilamoura, Portugal, 6–9 September 2008; pp. 1–6. [CrossRef]

5. Spadacini, G.; Grassi, F.; Pignari, S.A. Conducted emissions in the powertrain of electric vehicles. *IEEE Int. Symp. Electromagn. Compat.* **2017**, *69*, 1–15. [CrossRef]

6. Robles, E.; Fernandez, M.; Andreu, J.; Ibarra, E.; Ugalde, U. Advanced power inverter topologies and modulation techniques for common-mode voltage elimination in electric motor drive systems. *Renew. Sustain. Energy Rev.* **2021**, *140*, 110746. [CrossRef]

7. Plazenet, T.; Boileau, T.; Caironi, C.; Nahid-Mobarakeh, B. An overview of shaft voltages and bearing currents in rotating machines. In Proceedings of the IEEE Industry Application Society, 52nd Annual Meeting: IAS 2016, Portland, OR, USA, 2–6 October 2016; pp. 1–8. [CrossRef]

8. Robles, E.; Fernandez, M.; Ibarra, E.; Andreu, J.; Kortabarria, I. Mitigation of common mode voltage issues in electric vehicle drive systems by means of an alternative AC-decoupling power converter topology. *Energies* **2019**, *12*, 3349. [CrossRef]

9. Weber, T. EMC filters in high voltage traction drive systems. In Proceedings of the IEEE International Symposium on Electromagnetic Compatibility, Hamburg, Germany, 8–12 September 2008. [CrossRef]

10. Vostrov, K.; Pyrhonen, J.; Ahola, J. Shielding the end windings to reduce bearing currents. In Proceedings of the 2020 International Conference on Electrical Machines (ICEM), Gothenburg, Sweden, 23–26 August 2020; pp. 1431–1437. [CrossRef]

11. Mäki-ontto, P. Modeling and Reduction of Shaft Voltages in Ac Motors Fed By Frequency Converters. Ph.D. Thesis, Helsinki University of Technology, Esborg, Finland, 2006.

12. Zare, F. Practical approach to model electric motors for electromagnetic interference and shaft voltage analysis. *IET Electr. Power Appl.* **2010**, *4*, 727–738. [CrossRef]

13. Miloudi, H.; Bendaoud, A.; Miloudi, M.; Dickmann, S.; Schenke, S. Common mode and differential mode characteristics of AC motor for EMC analysis. In Proceedings of the IEEE International Symposium on Electromagnetic Compatibility, Wroclaw, Poland, 5–9 September 2016; pp. 765–769. [CrossRef]

14. Lee, S.; Liu, M.; Lee, W.; Sarlioglu, B. Comparison of High-Frequency Impedance of AC Machines with Circumferential and Toroidal Winding Topologies for SiC MOSFET Machine Drives. In Proceedings of the 2020 IEEE Energy Conversion Congress and Exposition (ECCE), Detroit, MI, USA, 11–15 October 2020; pp. 3572–3579. [CrossRef]

15. Xiong, Y.; Li, X.; Li, Y.; Zhao, X. A high-frequency motor model constructed based on vector fitting method. In Proceedings of the 2019 Joint International Symposium on Electromagnetic Compatibility, Sapporo and Asia-Pacific International Symposium on Electromagnetic Compatibility, EMC Sapporo/APEMC 2019, Sapporo, Japan, 3–7 June 2019; pp. 191–194. [CrossRef]

16. Xiong, Y.; Chen, X.; Zong, L.; Li, X.; Nie, X.; Yang, G.; Zhao, X. An Electric Drive System Modelling Method Based on Module Behavior. In Proceedings of the 2019 International Conference on Microwave and Millimeter Wave Technology, ICMMT 2019—Proceedings, Guangzhou, China, 19–22 May 2019; pp. 1–3. [CrossRef]

17. Gries, M.A.; Mirafzal, B. Permanent magnet motor-drive frequency response characterization for transient phenomena and conducted EMI analysis. In Proceedings of the 2008 Twenty-Third Annual IEEE Applied Power Electronics Conference and Exposition, Austin, TX, USA, 24–28 February 2008; pp. 1767–1775. [CrossRef]

18. Duan, Z.; Wen, X. A new analytical conducted EMI prediction method for SiC motor drive systems. *eTransportation* **2020**, *3*, 100047. [CrossRef]

19. Oganezova, I.; Kado, R.; Khvitia, B.; Kuchadze, Z.; Gheonjian, A.; Jobava, R. EMC model of low voltage DC motor. In Proceedings of the 2014 IEEE International Symposium on Electromagnetic Compatibility (EMC), Raleigh, NC, USA, 4–8 August 2014; pp. 81–85. [CrossRef]

20. Schinkel, M.; Weber, S.; Guttowski, S.; John, W.; Reichl, H. Efficient HF Modeling and Model Parameterization of Induction Machines for Time and Frequency Domain Simulations. In Proceedings of the Twenty-First Annual IEEE Applied Power Electronics Conference and Exposition, 2006. APEC '06, Dallas, TX, USA, 19–23 March 2006; Volume 2006, pp. 1181–1186. [CrossRef]

21. Cai, M.; Craddock, T.; Wasynczuk, O. High-frequency modeling, parameterization, and simulation of IPM motor drive systems. In Proceedings of the 2017 IEEE Power and Energy Conference at Illinois, PECI 2017, Champaign, IL, USA, 23–24 February 2017; pp. 1–8. [CrossRef]

22. Zhang, D.; Kong, L.; Wen, X.; Duan, Z. Interior permanent magnet motor drive system modeling for electromagnetic interference analysis. In Proceedings of the 2014 17th International Conference on Electrical Machines and Systems (ICEMS), Hangzhou, China, 22–25 October 2014; pp. 1498–1504. [CrossRef]

23. Hoffmann, A.; Ponick, B. Statistical Deviation of High-Frequency Lumped Model Parameters for Stator Windings in Three-Phase Electrical Machines. In Proceedings of the 2020 International Symposium on Power Electronics, Electrical Drives, Automation and Motion (SPEEDAM), Sorrento, Italy, 24–26 June 2020; pp. 85–90. [CrossRef]

24. Rahimi, A.; Kanzi, K. Improved High-Frequency Modeling of PMSM Using 3-D Finite Element Analysis. In Proceedings of the 2019 International Power System Conference (PSC), Tehran, Iran, 9–11 December 2019; pp. 71–78. [CrossRef]

25. Czuchra, W. Modelling of the Traction Induction Motor in the Frequency Band of Electromagnetic Conducted Disturbances. In Proceedings of the 2018 International Symposium on Electrical Machines (SME), Andrychow, Poland, 10–13 June 2018; pp. 1–4. [CrossRef]

26. Zhang, D.; Kong, L.; Wen, X. A measurement based modeling method of interior permanent magnet motor considering the rotor position for EMI analysis. In Proceedings of the IEEE Transportation Electrification Conference and Expo, ITEC Asia-Pacific 2014—Conference Proceedings, Beijing, China, 31 August–3 September 2014; pp. 1–6. [CrossRef]

27. Sun, J.; Xing, L. Parameterization of Three-Phase Electric Machine Models for EMI Simulation. *IEEE Trans. Power Electron.* **2014**, *29*, 36–41. [CrossRef]

28. Zhang, D.; Kong, L.; Wen, X. High frequency model of interior permanent magnet motor for EMI analysis. In Proceedings of the 2014 IEEE Conference and Expo Transportation Electrification Asia-Pacific (ITEC Asia-Pacific), Beijing, China, 31 August–3 September 2014; pp. 1–6. [CrossRef]

29. Boglietti, A.; Cavagnino, A.; Lazzari, M. Experimental high-frequency parameter identification of ac electrical motors. *IEEE Trans. Ind. Appl.* **2007**, *43*, 23–29. [CrossRef]

30. Carpaneto, A. Boglietti, E. An Accurate Induction Motor High-Frequency Model for Electromagnetic Compatibility Analysis. *Electr. Power Components Syst.* **2001**, *29*, 191–209. [CrossRef]

31. Pan, X.; Ehrhard, R.; Vick, R. An extended high frequency model of permanent magnet synchronous motors in hybrid vehicles. In Proceedings of the EMC Europe 2011 York—10th International Symposium on Electromagnetic Compatibility, York, UK, 26–30 September 2011; pp. 690–694.

32. Vidmar, G.; Miljavec, D. A Universal High-Frequency Three-Phase Electric-Motor Model Suitable for the Delta- and Star-Winding Connections. *IEEE Trans. Power Electron.* **2015**, *30*, 4365–4376. [CrossRef]

33. Mohammadi-Rostam, M.; Shahabi, M.; Shayegani-Akmal, A.A. High frequency lumped parameter model for EMI problems and over voltage analysis of Induction motor. *J. Electr. Eng.* **2013**, *13*, 278–283.

34. Gavrilenko, V.; Gavrilenko, V. Characterization of Winding Insulation of Electrical Machines Fed by Voltage Waves with High dV/dt. Ph.D. Thesis, Université Paris-Saclay, Université polytechnique de Tomsk (Russie), Gif-sur-Yvette, France, 2020.

35. Wu, Y.; Bi, C.; Jia, K.; Jin, D.; Li, H.; Yao, W.; Liu, G. High-frequency modelling of permanent magnet synchronous motor with star connection. *IET Electr. Power Appl.* **2018**, *12*, 539–546. [CrossRef]

36. Toulabi, M.S.; Wang, L.; Bieber, L.; Filizadeh, S.; Jatskevich, J. A Universal High-Frequency Induction Machine Model and Characterization Method for Arbitrary Stator Winding Connections. *IEEE Trans. Energy Convers.* **2019**, *34*, 1164–1177. [CrossRef]

37. Mirafzal, B.; Skibinski, G.L.; Tallam, R.M.; Schlegel, D.W.; Lukaszewski, R.A. Universal induction motor model with low-to-high frequency-response characteristics. *IEEE Trans. Ind. Appl.* **2007**, *43*, 1233–1246. [CrossRef]

38. Kane, M.; Ahmad, A.; Auriol, P. Multiwire Shielded Cable Parameter Computation. *IEEE Trans. Magn.* **1995**, *31*, 1646–1649. [CrossRef]

39. Radja, N.; Rachek, M.; Larbi, S.N. Improved RLMC-Circuit HF-Dependent Parameters Using FE-EM Computation Dedicated to Predict Fast Transient Voltage Along Insulated Windings. *IEEE Trans. Electromagn. Compat.* **2019**, *61*, 301–308. [CrossRef]

40. Guardado, J.L.; Cornick, K.J. Calculation of machine winding electrical parameters at high frequencies for switching transient studies. *IEEE Trans. Energy Convers.* **1996**, *11*, 33–40. [CrossRef]

41. Muetze, A.; Binder, A. Calculation of motor capacitances for prediction of the voltage across the bearings in machines of inverter-based drive systems. *IEEE Trans. Ind. Appl.* **2007**, *43*, 665–672. [CrossRef]

42. Ramos, J.I.; Dienot, J.M.; Vidal, P.E.; Viguier, C.; Nogarede, B. Contribution to modeling of parasitic couplings for predicting EMC behavior of electrical machines. In Proceedings of the 2014 International Conference on Electrical Machines (ICEM), Berlin, Germany, 2–5 September 2014; pp. 1056–1062. [CrossRef]

43. Ma, X.; Liu, R.; Zheng, B.; Zhang, Y. Analysis and calculation of capacitance parameters in induction machines to predict shaft voltage. In Proceedings of the ICEMS 2012 - Proceedings: 15th International Conference on Electrical Machines and Systems, Sapporo, Japan, 21–24 October 2012.

44. Benecke, J. Impedance and Emission Optimization of Low-Voltage DC Motors for EMC Compliance. *IEEE Trans. Ind. Electron.* **2011**, *58*, 3833–3839. [CrossRef]

45. Djukic, N.; Encica, L.; Paulides, J.J.H. Electrical machines: Comparison of existing analytical models and FEM for calculation of turn-to-turn capacitance in formed windings. In Proceedings of the 2016 Eleventh International Conference on Ecological Vehicles and Renewable Energies (EVER), Monte Carlo, Monaco, 6–8 April 2016; pp. 1–8. [CrossRef]

46. Djukic, N.; Encica, L.; Paulides, J.J.H. Electrical machines: Turn-to-turn capacitance in formed windings with rectangular cross-section wire. In Proceedings of the 2015 International Conference on Sustainable Mobility Applications, Renewables and Technology (SMART), Kuwait, Kuwait, 23–25 November 2015; pp. 1–4. [CrossRef]

47. Martis, C.; Hedesiu, H.; Tataranu, B. High-frequency model and conductive interferences of a small doubly salient permanent magnet machine. In Proceedings of the 2004 IEEE International Conference on Industrial Technology, 2004. IEEE ICIT '04, Hammamet, Tunisia, 8–10 December 2004; Volume 3, pp. 1378–1383. [CrossRef]

48. Maki-Ontto, P.; Luomi, J. Induction motor model for the analysis of capacitive and induced shaft voltages. In Proceedings of the IEEE International Conference on Electric Machines and Drives, San Antonio, TX, USA, 15 May 2005; pp. 1653–1660. [CrossRef]

49. Ferreira, J. Improved analytical modeling of conductive losses in magnetic components. *IEEE Trans. Power Electron.* **1994**, *9*, 127–131. [CrossRef]

50. Reddy, P.B.; Zhu, Z.Q.; Han, S.H.; Jahns, T.M. Strand-level proximity losses in PM machines designed for high-speed operation. In Proceedings of the 2008 18th International Conference on Electrical Machines, Vilamoura, Portugal, 6–9 September 2008; pp. 1–6. [CrossRef]

51. Magdun, O.; Binder, A.; Purcarea, C.; Rocks, A. High-frequency induction machine models for calculation and prediction of common mode stator ground currents in electric drive systems. In Proceedings of the 2009 13th European Conference on Power Electronics and Applications, EPE '09, Barcelona, Spain, 8–10 September 2009; pp. 1–8.

52. Mohammed, O.; Ganu, S.; Abed, N.; Liu, S.; Liu, Z. High frequency PM synchronous motor model determined by FE analysis. *IEEE Trans. Magn.* **2006**, *42*, 1291–1294. [CrossRef]

53. Vostrov, K.; Pyrhonen, J.; Ahola, J.; Niemela, M. Non-circulating Bearing Currents Mitigation Approach Based on Machine Stator Design Options. In Proceedings of the 2018 23rd International Conference on Electrical Machines, ICEM 2018, Alexandroupoli, Greece, 3–6 September 2018; pp. 866–872. [CrossRef]

54. Kwack, Y.; Kim, H.; Song, C.; Moon, M.; Kim, D.H.; Kim, B.; Kim, E.; Kim, J. EMI modeling method of interior permanent magnet synchronous motor for hybrid electric vehicle drive system considering parasitic and dynamic parameters. In Proceedings of the 2015 Asia-Pacific Symposium on Electromagnetic Compatibility (APEMC), Taipei, Taiwan, 26–29 May 2015; pp. 78–81. [CrossRef]

55. Kohji, M.; Hiroki, F.; Liang, S. Motor modeling for EMC simulation by 3-D electromagnetic field analysis. In Proceedings of the 2009 IEEE International Electric Machines and Drives Conference, Miami, FL, USA, 3–6 May 2009; pp. 103–108. [CrossRef]

56. Mohammed, O.A.; Ganu, S. FE-Circuit Coupled Model of Electric Machines for Simulation and Evaluation of EMI Issues in Motor Drives. *IEEE Trans. Magn.* **2010**, *46*, 3389–3392. [CrossRef]

57. Sangha, P.; Sawata, T. Evaluation of winding stray capacitance in motors for aerospace applications. In Proceedings of the 2017 IEEE International Electric Machines and Drives Conference (IEMDC), Miami, FL, USA, 21–24 May 2017; pp. 1–6. [CrossRef]

58. Heidler, B.; Brune, K.; Doppelbauer, M. High-frequency model and parameter identification of electrical machines using numerical simulations. In Proceedings of the 2015 IEEE International Electric Machines & Drives Conference (IEMDC), Coeur d'Alene, ID, USA, 10–13 May 2015; pp. 1221–1227. [CrossRef]

59. Mohammed, O.A.; Ganu, S.; Liu, S.; Liu, Z.; Abed, N. Study of high frequency model of permanent magnet motor. In Proceedings of the 2005 IEEE International Conference on Electric Machines and Drives, San Antonio, TX, USA, 15 May 2005; pp. 622–627. [CrossRef]

60. Ferreira, R.S.; Ferreira, A.C. Transient Voltage Distribution in Induction Motor Stator Windings Using Finite Elements Method. In Proceedings of the IECON 2018—44th Annual Conference of the IEEE Industrial Electronics Society, Washington, DC, USA, 21–23 October 2018; pp. 737–742. [CrossRef]

61. Ferreira, R.S.; Ferreira, A.C. Transient model to study voltage distribution in electrical machine windings considering the rotor. *Electr. Power Syst. Res.* **2021**, *195*, 107155. [CrossRef]

62. Jaritz, M.; Stieger, N.; Jaeger, C.; Schneider, M.; Vukovic, D.; Blume, S.; Smajic, J. An Improved Model for the Common Mode Impedance in Inverter-Fed AC Machines. In Proceedings of the 2020 International Conference on Electrical Machines (ICEM), Gothenburg, Sweden, 23–26 August 2020; pp. 1053–1059. [CrossRef]

63. De Gersem, H.; Henze, O.; Weiland, T.; Binder, A. Transmission-line modelling of wave propagation effects in machine windings. In Proceedings of the 2008 13th International Power Electronics and Motion Control Conference, Poznan, Poland, 1–3 September 2008; pp. 2385–2392. [CrossRef]

64. Zhang, J.; Xu, W.; Gao, C.; Wang, S.; Qiu, J.; Zhu, J.G.; Guo, Y. Analysis of inter-turn insulation of high voltage electrical machine by using multi-conductor transmission line model. *IEEE Trans. Magn.* **2013**, *49*, 1905–1908. [CrossRef]

65. Sarrio, J.E.R.; Martis, C.; Chauvicourt, F. Numerical Computation of Parasitic Slot Capacitances in Electrical Machines. In Proceedings of the 2020 International Conference and Exposition on Electrical And Power Engineering (EPE), Iasi, Romania, 22–23 October 2020; pp. 146–150. [CrossRef]

66. Birnkammer, F.; Chen, J.; Pinhal, D.B.; Gerling, D. Influence of the Modeling Depth and Voltage Level on the AC Losses in Parallel Conductors of a Permanent Magnet Synchronous Machine. *IEEE Trans. Appl. Supercond.* **2018**, *28*, 1–5. [CrossRef]

67. Brauer, P. High-Frequency Voltage Distribution Modelling of a Slotless PMSM from a Machine Design Perspective. Ph.D. Thesis, Kth Royal Institute of Technology, Stockholm, Sweden, 2018.

68. Venegas, V.; Guardado, J.L.; Melgoza, E.; Hernandez, M. A finite element approach for the calculation of electrical machine parameters at high frequencies. In Proceedings of the 2007 IEEE Power Engineering Society General Meeting, Tampa, FL, USA, 24–28 June 2007. [CrossRef]

69. Krings, A.; Paulsson, G.; Sahlen, F.; Holmgren, B. Experimental investigation of the voltage distribution in form wound windings of large AC machines due to fast transients. In Proceedings of the 2016 22nd International Conference on Electrical Machines, ICEM 2016, Lausanne, Switzerland, 4–7 September 2016; pp. 1700–1706. [CrossRef]

70. Ruiz-Sarrio, J.E.; Chauvicourt, F.; Gyselinck, J.; Martis, C. High-Frequency Modelling of Electrical Machine Windings Using Numerical Methods. In Proceedings of the 2021 IEEE International Electric Machines & Drives Conference (IEMDC), Hartford, CT, USA, 17–20 May 2021; pp. 1–7. [CrossRef]

71. Volpe, G.; Popescu, M.; Marignetti, F.; Goss, J. AC winding losses in automotive traction e-machines: A new hybrid calculation method. In Proceedings of the 2019 IEEE International Electric Machines and Drives Conference, IEMDC 2019, San Diego, CA, USA, 12–15 May 2019; pp. 2115–2119. [CrossRef]

72. Taran, N.; Ionel, D.M.; Rallabandi, V.; Heins, G.; Patterson, D. An Overview of Methods and a New Three-Dimensional FEA and Analytical Hybrid Technique for Calculating AC Winding Losses in PM Machines. *IEEE Trans. Ind. Appl.* **2021**, *57*, 352–362. [CrossRef]

73. Jaritz, M.; Jaeger, C.; Bucher, M.; Smajic, J.; Vukovic, D.; Blume, S. An Improved Model for Circulating Bearing Currents in Inverter-Fed AC Machines. In Proceedings of the 2019 IEEE International Conference on Industrial Technology (ICIT), Melbourne, VIC, Australia, 13–15 February 2019; pp. 225–230. [CrossRef]

74. CISPR. *Guidance for Users of the CISPR Standards*; Technical Report; International Electrotechnical Commission International Special Committee on Radio Interference (CISPR): Geneva, Switzerland, 2015.

75. Zhao, H.; Yao, J.; Wang, S. A Universal DM/CM Physical Model for Power Transformer EMI Analysis within both Conducted and Radiated Frequency Ranges. In Proceedings of the 2018 IEEE Energy Conversion Congress and Exposition (ECCE), Portland, OR, USA, 23–27 September 2018; pp. 6592–6599. [CrossRef]

76. Kim, S.; Neikirk, D.P. Compact equivalent circuit model for the skin effect. *IEEE MTT-S Int. Microw. Symp. Dig.* **1996**, *3*, 1815–1818. [CrossRef]

77. Idir, N.; Weens, Y.; Franchaud, J.J. Skin effect and dielectric loss models of power cables. *IEEE Trans. Dielectr. Electr. Insul.* **2009**, *16*, 147–154. [CrossRef]

78. Al-Timimy, A.; Giangrande, P.; Degano, M.; Galea, M.; Gerada, C. Investigation of AC Copper and Iron Losses in High-Speed High-Power Density PMSM. In Proceedings of the 2018 XIII International Conference on Electrical Machines (ICEM), Alexandroupoli, Greece, 3–6 September 2018; pp. 263–269. [CrossRef]

79. Stockbrügger, J.O.; Ponick, B. Analytical determination of the end-winding portion of the winding-to-rotor capacitance for the prediction of bearing voltage in electrical machines. *Electr. Eng.* **2020**, *102*, 2481–2491. [CrossRef]

80. Ceraolo, M.; Poli, D. *Fundamentals of Electric Power Engineering*; John Wiley & Sons, Inc.: Hoboken, NJ, USA, 2014; pp. 20–36. [CrossRef]

81. Fleisch, D. *A Student's Guide to Maxwell's Equations*, 1st ed.; Cambridge University Press: New York, NY, USA, 2008.

82. Zhao, H.; Eldeeb, H.H.; Zhang, Y.; Zhang, D.; Zhan, Y.; Xu, G.; Mohammed, O.A. An Improved Core Loss Model of Ferromagnetic Materials Considering High-Frequency and Non-Sinusoidal Supply. *IEEE Trans. Ind. Appl.* **2021**, *9994*, 1. [CrossRef]

83. Smajic, J.; Bucher, M.; Franz, T.; Cranganu-Cretu, B.; Shoory, A.; Tepper, J. Modeling of Frequency Dependent Parameters in Time Domain High Frequency Transformer Simulations. *Procedia Eng.* **2017**, *202*, 251–263. [CrossRef]

84. Winterborne, D.; Jordan, S.; Sjoberg, L.; Atkinson, G. Estimation of AC copper loss in electrical machine windings with consideration of end effects. In Proceedings of the 2020 International Conference on Electrical Machines (ICEM), Gothenburg, Sweden, 23–26 August 2020; pp. 847–853. [CrossRef]

85. Jaeger, C.; Grinbaum, I.; Smajic, J. Numerical simulation and measurement of common-mode and circulating bearing currents. In Proceedings of the 2016 XXII International Conference on Electrical Machines (ICEM), Lausanne, Switzerland, 4–7 September 2016; pp. 486–491. [CrossRef]

86. Mohammed, O.A.; Ganu, S.; Abed, N.; Liu, Z.; Liu, S. High frequency modeling of PM synchronous machine for use in integrated motor drive. In Proceedings of the IEEE Electric Ship Technologies Symposium, ESTS 2007, Arlington, VA, USA, 21–23 May 2007; pp. 245–249. [CrossRef]

87. Mahdavi, S.; Hameyer, K. High frequency equivalent circuit model of the stator winding in electrical machines. In Proceedings of the Proceedings—2012 20th International Conference on Electrical Machines, ICEM 2012, Marseille, France, 2–5 September 2012; pp. 1706–1711. [CrossRef]

88. Rincón, D.; Aguilera, E.; Chacón, J.C. Numerical treatment of floating conductors based on the traditional finite element formulation. *Adv. Electromagn.* **2018**, *7*, 46–55. [CrossRef]

89. Dowell, P. Effects of eddy currents in transformer windings. *Proc. Inst. Electr. Eng.* **1966**, *113*, 1387. [CrossRef]

90. Electric Machinery Committee. *IEEE Standard Test Procedure for Polyphase Induction Motors and Generators*; Technical Report 4; IEEE: Piscataway, NJ, USA, 2018. [CrossRef]

91. Djukic, N.; Encica, L.; Paulides, J.J.H. Overview of capacitive couplings in windings. In Proceedings of the 2015 Tenth International Conference on Ecological Vehicles and Renewable Energies (EVER), Monte Carlo, Monaco, 31 March–2 April 2015; pp. 1–11. [CrossRef]

92. Massarini, A.; Kazimierczuk, M. Self-capacitance of inductors. *IEEE Trans. Power Electron.* **1997**, *12*, 671–676. [CrossRef]

93. Yang, Y.M.; Peng, H.M.; Wang, Q.D. Common Model EMI Prediction in Motor Drive System for Electric Vehicle Application. *J. Electr. Eng. Technol.* **2015**, *10*, 205–215. [CrossRef]

94. Almandoz, G.; Zarate, S.; Egea, A.; Moreno, Y.; Urdangarin, A.; Moreno, R. High Frequency Modeling of Electric Drives for Electromagnetic Compatibility Analysis. In Proceedings of the 2020 International Conference on Electrical Machines (ICEM), Gothenburg, Sweden, 23–26 August 2020; pp. 1129–1135. [CrossRef]

95. Abdallah, F. EMC Analysis of Electric Drives. Ph.D. Thesis, LUND University, Lund, Sweden, 2012.

96. Popov, M. General approach for accurate resonance analysis in transformer windings. *Electr. Power Syst. Res.* **2018**, *161*, 45–51. [CrossRef]
97. Zhao, X.; Yao, C.; Abu-Siada, A.; Liao, R. High frequency electric circuit modeling for transformer frequency response analysis studies. *Int. J. Electr. Power Energy Syst.* **2019**, *111*, 351–368. [CrossRef]
98. Boucenna, N.; Hlioui, S.; Revol, B.; Costa, F. A detailed analysis of the propagation paths of high-frequency common mode currents in AC motors. In Proceedings of the 2013 15th European Conference on Power Electronics and Applications, EPE 2013, Lille, France, 2–6 September 2013. [CrossRef]
99. Mellor, P.; Wrobel, R.; McNeill, N. Investigation of Proximity Losses in a High Speed Brushless Permanent Magnet Motor. In Proceedings of the Conference Record of the 2006 IEEE Industry Applications Conference Forty-First IAS Annual Meeting, Tampa, FL, USA, 8–12 October 2006; Volume 3, pp. 1514–1518. [CrossRef]
100. Kovacova, I.; Melnykov, V. Magnetic Fields of DC PM Motor and its EMC. In Proceedings of the International Conference on Modern Electrical and Energy Systems, MEES 2019, Kremenchuk, Ukraine, 23–25 September 2019; pp. 186–189. [CrossRef]
101. Taran, N.; Rallabandi, V.; Ionel, D.M.; Zhou, P.; Thiele, M.; Heins, G. A Systematic Study on the Effects of Dimensional and Materials Tolerances on Permanent Magnet Synchronous Machines Based on the IEEE Std 1812. *IEEE Trans. Ind. Appl.* **2019**, *55*, 1360–1371. [CrossRef]

Short Biography of Authors

Yerai Moreno was born in Irún, Spain in 1996. He received the B.Sc. degree in electrical engineering from the University of the Basque Country, Donostia-San Sebastian, Spain in 2018 and the M.S. degree in industrial engineering from Mondragon Uniberstitatea, Arrasate, Spain, in 2020. Since 2018, he has been with the Electronics and Computing Department, Faculty of Engineering, Mondragon Unibertsitatea, where he is currently pursuing the Ph.D. degree. His current research interest includes permanent-magnet machine design, modeling and EMC optimization of electric drives.

Gaizka Almandoz (M'04) was born in Arantza, Spain. He received the B.Sc. and Ph.D. degrees in electrical engineering from Mondragon Unibertsitatea, Mondragon, Spain, in 2003 and 2008, respectively. Since 2003, he has been with the Electronics and Computing Department, Faculty of Engineering, Mondragon Unibertsitatea, where he is currently an Associate Professor. His current research interest includes electrical machine design, modeling, and control. He has participated in various research projects in the fields of wind energy systems, elevator drive, and railway traction.

Aritz Egea received the degree in electrical engineering from the University of Mondragon, Mondragon, Spain, in 2009, and the Ph.D. degree in electrical engineering in 2012. He is currently an Associate Professor at the Faculty of Engineering, Mondragon Unibertsitatea. His current research interests include electrical machine design and control and electromagnetic actuators.

Beñat Arribas was born in Idiazabal, Basque Country, Spain, in 1998. He received his B.Sc. degree in electronics engineering from Mondragon Unibertsitatea in 2020 where he is currently pursuing the M.Sc. degree in energy and power electronics. He is also collaborating with the Electric Energy research group of Mondragon Unibertsitatea since 2017 in the field of drive systems applied to traction and the generation of electric energy. His current research interests include electrical machine analysis, design and control.

Ander Urdangarin was born in Ordizia. Spain, in February 1982. He received the B.Sc. degree in Automatic and industrial electronics from Mondragon Unibertsitatea, Mondragon, Spain, in 2009. Between 2010–2012, he was with the Department of Electronics, Faculty of Engineering of Mondragon Unibertsitatea. Since 2012 he is member of ORONA. His current research interests include power electronics design, modeling, and control.